Science of the Total Environment 816 (2022) 151532

Contents lists available at ScienceDirect

Science of the Total Environment

journal homepage: www.elsevier.com/locate/scitotenv

Biotic and abiotic reductive dechlorination of chloroethenes in aquitards

Diana Puigserver [a,*], Jofre Herrero [b], Xènia Nogueras [c,f], Amparo Cortés [d], Beth L. Parker [e], E. Playà [c], José M. Carmona [b]

[a] Department of Mineralogy, Petrology and Applied Geology, Faculty of Earth Sciences, University of Barcelona (UB), Water Research Institute (IdRA-UB), Serra Húnter Tenure-elegible Lecturer, C/ Martí i Franquès, s/n, E-08028 Barcelona, Spain
[b] Department of Mineralogy, Petrology and Applied Geology, Faculty of Earth Sciences, University of Barcelona (UB), Water Research Institute (IdRA-UB). C/ Martí i Franquès, s/n, E-08028 Barcelona, Spain
[c] Department of Mineralogy, Petrology and Applied Geology, Faculty of Earth Sciences, University of Barcelona (UB). C/ Martí i Franquès, s/n, E-08028 Barcelona, Spain
[d] Department of Biology, Health and Environment, Faculty of Pharmacy, University of Barcelona, Av. Joan XXIII, 27-31, E-08028 Barcelona, Spain
[e] School of Engineering, University of Guelph, 50, Stone Road East, Guelph, N1G 2W1, Ontario, Canada
[f] Health Section of the City Council of Mataró (Barcelona), Specialized Support Technician, Carrer de la Riera, 48, 08301 Mataró, Barcelona, Spain

HIGHLIGHTS

- Chloroethenes degradation in aquitards occurs mainly in the matrix near fractures.
- Parent and metabolite haloes in matrix and isotopic fractioning reveal degradation.
- Textural changes favor microbial development and give rise to ecotones.
- Dimethylacetamide, as a new trap, serves to measure $\delta^{13}C$ of matrix chloroethenes.
- Coupling of abiotic and biotic degradation of PCE and TCE in the matrix occurs.

GRAPHICAL ABSTRACT

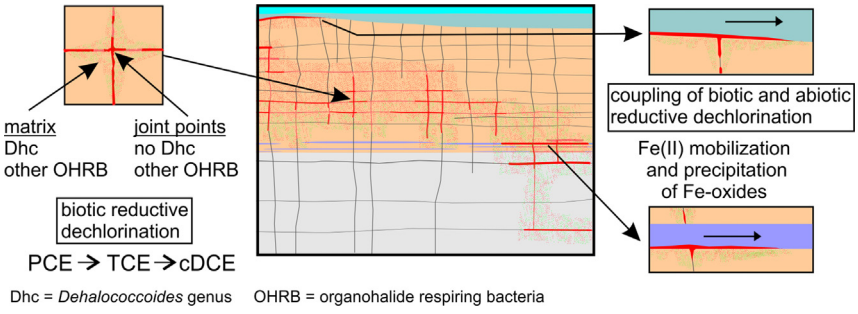

ARTICLE INFO

Article history:
Received 7 April 2021
Received in revised form 3 November 2021
Accepted 4 November 2021
Available online 6 November 2021

Editor: José Virgílio Cruz

Keywords:
Reductive dechlorination
Joint-point
Dehalococcoides
Propionibacterium acnes
Ecotone
Iron oxides

ABSTRACT

Chlorinated solvents occur as dense nonaqueous phase liquid (DNAPL) or as solutes when dissolved in water. They are present in many pollution sites in urban and industrial areas. They are toxic, carcinogenic, and highly recalcitrant in aquifers and aquitards. In the latter case, they migrate by molecular diffusion into the matrix. When aquitards are fractured, chlorinated solvents also penetrate as a free phase through the fractures. The main objective of this study was to analyze the biogeochemical processes occurring inside the matrix surrounding fractures and in the joint-points zones. The broader implications of this objective derive from the fact that, incomplete natural degradation of contaminants in aquitards generates accumulation of daughter products. This causes steep concentration gradients and back-diffusion fluxes between aquitards and high hydraulic conductivity layers. This offers opportunities to develop remediation strategies based, for example, on the coupling of biotic and reactive abiotic processes. The main results showed: 1) Degradation occurred especially in the matrix adjacent to the orthogonal network of fractures and textural heterogeneities, where texture contrasts favored microbial development because these zones constituted ecotones. 2) A dechlorinating bacterium not belonging to the *Dehalococcoides* genus, namely *Propionibacterium acnes*, survived under the high concentrations of dissolved perchloroethene (PCE) in contact with the PCE-DNAPL and was able to degrade it to trichloroethene (TCE). *Dehalococcoides* genus was able to conduct PCE reductive dechlorination at least up to cis-1,2-dichloroethene (cDCE), which shows again the potential of the medium to degrade chloroethenes in aquitards.

* Corresponding author.
E-mail addresses: puigserverdiana@ub.edu (D. Puigserver), jofreherreroferran@ub.edu (J. Herrero), xnogueras@ajmataro.cat (X. Nogueras), acortes@ub.edu (A. Cortés), bparker@uoguelph.ca (B.L. Parker), eplaya@ub.edu (E. Playà), jmcarmona@ub.edu (J.M. Carmona).

https://doi.org/10.1016/j.scitotenv.2021.151532

3) Degradation of PCE in the matrix resulted from the coupling of reactive abiotic and biotic processes—in the first case, promoted by Fe^{2+} sorbed to iron oxides, and in the latter case, related to dechlorinating microorganisms. The dechlorination resulting from these coupling processes is slow and limited by the need for an adequate supply of electron donors.

1. Introduction

Chloroethenes are chlorinated solvents that have been used for many purposes, among them: metal cleaning and degreasing; cold and dry cleaning of textile products; degreasing of leather and wool; extraction of seed oils; removal of paints, lacquers, varnishes, waxes, and resins; manufacturing of adhesives, aerosols, phenol, aniline, insecticides, and dyes; intermediates in manufacturing chemical products; electronics; dielectric fluids; and heat transfer medium (Pankow and Cherry, 1996). They are dense non-aqueous phase liquids (DNAPLs) that are present in numerous pollution episodes associated with urban and industrial areas (Yu et al., 2015). Among their physicochemical characteristics, their low biodegradability under natural attenuation conditions stands out (Field and Sierra-Alvarez, 2004). Moreover, their variable hydrophobicity (Cwiertny and Scherer, 2010) conditions their sorption on soil materials. All of these factors have led them to become organic compounds that last in the environment for long periods of time (several decades or more; Pankow and Cherry, 1996). These compounds are carcinogenic (Yadav and Pandey, 2018), and their presence in soil and groundwater puts human health and ecosystems at risk (Cheng et al., 2016). Hence, their maximum permissible levels in both water and soil are regulated. In some cases, these levels are very low (USEPA, 2004). Indeed, the European guidelines on drinking water establish that the sum of perchloroethene (PCE) and trichloroethene (TCE) should not exceed 10 μg/L. The threshold values of PCE and TCE in contaminated soils for human health protection in industrial, urban, and other use areas are 10.0, 1.0, and 0.1, respectively for PCE; and 70.0, 7.0, and 0.7, respectively, for TCE (all values in mg/kg dry weight).

The force of gravity governs the DNAPL free phase migration through the soil (Scheutz et al., 2011), while the relative mobility of DNAPLs with respect to groundwater is controlled by the density/viscosity ratio of DNAPLs and groundwater (Cheremisinoff, 2017). In the subsurface, DNAPL may be distributed in different physical states known as phases. The concentration in each phase is described by the classical model of the Four Phase System (Huling and Weaver, 1991). According to this model, each contaminant constituting the DNAPL can be distributed among any or all of the following four phases with a determined equilibrium concentration: i) Air phase, as contaminants may occur as vapors in the unsaturated zone; ii) Soil phase, as contaminants may be adsorbed onto solid subsurface materials; iii) Water phase, as contaminants may be dissolved in water depending on their solubility; and iv) Immiscible liquid phase, as contaminants also exist as DNAPL. The distribution of a DNAPL contaminant between these phases can be described by empirical relationships known generically as partition coefficients, which are largely site-specific and largely depend on the physicochemical characteristics of both the DNAPL and environmental matrices in the subsurface porous medium. These coefficients allow the calculation of the equilibrium concentrations between the phase pairs (Huling and Weaver, 1991).

One of the granular contexts where chloroethenes are most recalcitrant are aquitards, formed by sediments of low hydraulic conductivity (K), such as clays, silts, and fine sands (Dearden et al., 2013). Aquitards, whether or not they outcrop at the ground surface, may form the top and bottom of confined or semiconfined aquifers. They may also form the bottom of unconfined aquifers. Furthermore, they may be located between the unsaturated zone and the water table of unconfined aquifers.

Aquitards are often fractured, allowing migration of DNAPLs through the fracture network; this ability substantially increases the vulnerability of the underlying aquifer units (Fjordbøge et al., 2017). These fractures constitute preferential migration pathways of the free phase of chlorinated solvents and often lead to the contamination of the underlying aquifers. This free phase penetration into the aquitard takes place by two mechanisms. The first is the capillary flow along the fractures, given the low interfacial tension of these liquids and the very small fracture opening sizes (up to only 10 μm; Walton et al., 2019). The second mechanism is the gravity flow along fractures following the so-called cubic law, which is directly proportional to the K value along the fracture (Fang and Zhu, 2018). In the case of free phase chlorinated solvent DNAPLs, they are denser and usually less viscous than water, and thus the resulting K values are higher for free phase DNAPLs than for water (O'hara et al., 2000).

In clays, silts, and fine sands, the volume of void spaces that constitute the total porosity of the matrix is quite high, with values for this parameter ranging from 26% to 60% (Domenico and Schwartz, 1998). Grain size controls whether the transport in a porous media is dominated by molecular diffusion or advection (through finer or coarser materials, respectively). Forward diffusion through fine materials (clays, silts, or fine sands; Brown et al., 2012) leads to a significant amount of the contaminant mass that circulates as the dissolved phase through the fractures; it migrates into the matrix surrounding those fractures (Parker et al., 1994; Huang and Goltz, 2015). This contaminant mass remains either sorbed onto that matrix (Scheutz et al., 2010) or as a dissolved phase in the porewater occupying the porosity (Sale et al., 2008). This mass of contaminants thereby acts as a long-term source of contamination when back-diffusion occurs because of the reversal of the concentration gradient between aquifer and aquitard when remediation or removal of sources has been completed (Chapman et al., 2012; Yang et al., 2017).

The thin, more conductive layers in the transition zone to bottom aquitards (Puigserver et al., 2013, 2016a, 2016b) also play a key role in biodegradation of chlorinated solvents, for example, under anoxic conditions. The continuous groundwater flow through these conductive layers supplies the less conductive layers where contaminants accumulate with several components: electron acceptors (e.g., dissolved oxygen [DO]) and donors (e.g., dissolved organic matter [DOM]), nutrients, and other substances that microorganisms need to live. Biogeochemical processes leading to the oxidation of DOM and the depletion of DO lead to biotic reductive dechlorination of chlorinated solvents when dominant redox conditions become sufficiently reducing (Wiedemeier et al., 1998; Bradley, 2003, 2011). The fracture zones that affect aquitards play a similar role to the mentioned conductive layers.

Although natural attenuation of chloroethenes occurs spontaneously in anoxic environments at low degradation rates, it is possible to stimulate this process to attain their complete in situ mineralization (Van Agteren et al., 1998). Biotic reductive dechlorination is the dominant process for the natural biodegradation of the most highly chlorinated chloroethenes (Weatherill et al., 2018). Thus, PCE is the most prone to reductive dechlorination because it is more oxidized than the other chloroethenes. For the same reason, the decline in reductive dechlorination is caused by a decrease in the energy that can be gained from the metabolic transformation of the less oxidated chloroethenes (Vogel and McCarty, 1985; Bouwer, 1994), that is, as the number of chlorine atoms decreases. Biotic reductive dechlorination represents

anaerobic respiration that is mostly carried out by organohalide-respiring bacteria. Reductive dechlorination of PCE has been described as a sequential reaction that generates increasingly lighter metabolites, from PCE to the harmless ethene or ethane (Jugder et al., 2016). However, this process is often incomplete, and thus cDCE and vinyl chloride (VC) accumulate in aquifers and aquitards (Puigserver et al., 2016a). This incomplete reductive dechlorination increases the risk to human health and ecosystems because these compounds are more toxic than the parents from which they originate (Dolinová et al., 2017).

Reductive dechlorination occurs in different redox zones. For example, reductive dechlorination from PCE to TCE can be initiated under denitrification conditions (Chapelle and Bradley, 2004; Weatherill et al., 2019), the change from TCE to cDCE under manganese (Mn)- and iron (Fe)-reducing conditions (Němeček et al., 2020), the shift from cDCE to VC under sulfate-reducing conditions (Antoniou et al., 2019), and the shift from VC to ethene and ethane under methanogenic conditions (Herrero et al., 2019). In the case of prevailing oxidizing conditions, cDCE and VC can be oxidized (Field and Sierra-Alvarez, 2001; Findlay et al., 2016).

Among the genera of microorganisms responsible for the reductive dechlorination of halogenated aliphatic compounds are *Desulfitobacterium* and *Clostridium* and, within the genus *Dehalobacter*, the species *Dehalobacter restrictus* (Kim et al., 2006). Only some strains of the *Dehalococcoides* genus are capable of performing complete reductive dechlorination (Saiyari et al., 2018). The presence of these strains can be used as a proxy for the occurrence of organohalide respiration. Within this genus, the species *Dehalococcoides mccartyi* has been described as able to mineralize PCE (Löffler et al., 2013). This microorganism has been detected in contaminated sites where anaerobic niches occur, such as those studied by Krzmarzick et al. (2012). Moreover, Chang et al. (2011) described that several strains of *Propionibacterium* genus (*Propionibacterium* sp. strain HK-1 and *Propionibacterium acnes* strain HK-3,) were able to dechlorinate PCE under anaerobic conditions by dehalorespiration without accumulation of toxic intermediates.

Oxidizing dehalogenators have also been identified, among which are aerobic microorganisms that can oxidize chloroethenes to carbon dioxide (CO_2), such as methylotrophs (Semprini, 1997), methanol oxidizers (Fitch et al., 1996), ethene oxidizers (Verce et al., 2001), propane oxidizers (Malachowsky et al., 1994), propene oxidizers (Reij et al., 1995), isopropene oxidizers (McCarty, 1997), aromatic compound oxidizers (e.g., toluene, Shim et al., 2001), ammonium oxidizers, and VC oxidizers (Verce et al., 2002).

Abiotic degradation of chloroethenes has been described in natural contexts, especially in the presence of Fe minerals such as pyrite, troilite, mackinawite, vivianite (Bae and Lee, 2012), magnetite (Culpepper et al., 2018), Fe^{2+} sorbed to iron oxides, Fe^{2+}-containing clay minerals, and even biotite (He et al., 2015) and green rust (He et al., 2015; Fan et al., 2016; Puigserver et al., 2020). The interdependence between reactive abiotic and biotic processes may favor a coupling between both processes and may lead to a higher rate of degradation of chlorinated solvents (Berns et al., 2019; Puigserver et al., 2020).

It is well known that high concentrations of chloroethenes in the contaminant source can inhibit microbial activity (National Research Council, 1999). However, laboratory studies by Nielsen and Keasling (1999) and Yang and McCarty (2000) have shown that some cultures can lead to PCE reductive dechlorination even at saturation concentrations. Furthermore, these studies have shown that the presence of dechlorination activity can significantly increase the dissolution rate of the PCE source (Yang and McCarty, 2002). In addition, high concentrations of chloroethenes can inhibit the activity of other microorganisms that compete with those that carry out reductive dehalogenation, such as methanogenic microorganisms (Yang and McCarty, 2002). Other studies, such as those conducted by Popat and Deshusses (2011) and Sabalowsky and Semprini (2010), have shown how the inhibition of microorganisms of the *Dehalococcoides* genus in degrading cDCE and VC, in the presence of high concentrations of parent chloroethenes, is a function of the presence of certain enzymes, as well as the exogenous supply of corrinoids, such as vitamin B12 (cyanocobalamin), which act as an essential cofactor for reductive dehalogenases (McMurdie et al., 2009).

Because aquitards are low-permeability formations, no wells can be installed like in groundwater systems. Therefore, intensive subsampling of borehole cores is essential in aquitards to determine the depth distribution of the contaminants and their isotopic composition in the porewater. Regarding the isotopic fractionation of chlorinated solvents in low-permeability formations, Wanner et al. (2017) studied the isotopic fractionation that occurs in these compounds by the processes of molecular diffusion and sorption on organic matter in these types of formations. These authors showed that these two processes overlap and compensate for each other to some extent, as they fractionate isotopes in the opposite directions. They established the value of 2‰ isotope fractionation shift as a threshold above which it is possible to unequivocally attribute part of the isotope fractionation observed in low-permeability formations to biodegradation or abiotic degradation processes other than molecular diffusion or sorption.

Subsampling is also necessary to study the biogeochemical conditions under which biodegradation processes occur in the subsurface (Parker et al., 2003). Because water monitoring in aquitards is often difficult, sampling porewater is a particularly useful tool (Adamson et al., 2015). This is noteworthy in the case of fractured aquitards, especially when analyzing the distribution of contaminants (and their mass) in the matrix of the sediment surrounding each single fracture, and in the fracture plane (Rivett et al., 2014). In fact, despite the apparent homogeneity of aquitards, fracture zones require a thorough characterization because they become anomalous zones, due to the presence of contaminants and the biogeochemical processes occurring in them (Damgaard et al., 2013). Moreover, the existence of fractures and coarse-grained interbedded layers confers a certain heterogeneity to these aquitards. These fracture zones and levels with different grain sizes and textural changes are accompanied by high microbial diversity and/or the presence of more developed microbial communities (Goldscheider et al., 2006; Herrero et al., 2021c). Hence, these zones become true ecotones within the aquitards, as described by Puigserver et al. (2013).

The novelty of the study lies on the role of the internal geological and hydrogeological structures of the aquitards related to the biotic and abiotic processes capable of degrading chlorinated solvents. To date, the scientific literature on the degradation processes of these compounds in aquitards has not studied the role played by the heterogeneities that constitute the mentioned internal structures occurring in these hydrogeological formations, which highlights the novelty of our study. In particular, the internal geological structures of aquitards important for the degradation of chlorinated solvents are of two types. Firstly, stratification and sedimentation patterns giving rise to textural subhorizontal heterogeneities at different depths within the aquitards. These patterns are bedding planes and texture contrasts between adjacent layers of fine and coarse grain sizes (such as thin interbedded layers of coarse sands or fine to medium gravels). Secondly, a dense system of subvertical microfractures that constitute subvertical heterogeneities. These microfractures are discontinuities that intersect the previous sedimentary structures giving rise to an orthogonal network of textural heterogeneities. The maximum textural contrast is found in three situations where the aquitard matrix is in geological contact with joint-point zones, subvertical microfractures, and along the contact with coarser grain size layers. In turn, this network gives rise to a network of hydraulic conductivity contrasts, which conforms the internal hydrogeological structures within aquitards. This allows DNAPL to migrate as a free phase through the aquitards and penetrate by molecular diffusion into the surrounding matrix. Degradation occurs especially in the matrix surrounding the heterogeneities, where texture contrasts favor microbial development and diversity, as these zones become ecotones within aquitards. Parent compounds, such as PCE, and daughter products

degrade because of the coupling of biodegradation and reactive abiotic processes promoted by iron oxides present in the matrix (Weathers and Parkin, 1995; Bradley and Chapelle, 1997; Lee et al., 1998; Puigserver et al., 2016b; Hua et al., 2021). This shows the potential of the medium to degrade chlorinated solvents in aquitards. The identification of the mentioned heterogeneities is important to a priori determine the depths at which chlorinated solvents are located and the extent to which their natural degradation (often incomplete) is occurring (Puigserver et al., 2020), as it is at these depths where remediation systems should focus efforts on enhancing dechlorination until complete mineralization at this and other sites.

Two working hypotheses were formulated. i) In aquitards, the presence of microorganisms and minerals acting as electron donors, together with the existence of fairly constant physicochemical conditions, favors reactive abiotic and biotic reductive dechlorination, especially in the matrix adjacent to fractures. ii) The existence of textural heterogeneities formed by fractures that cross aquitards and by interbedded layers of coarser grain size significantly favor the presence of microorganisms that contribute to the biogeochemical processes of chloroethene degradation.

To test these hypotheses, a field site on a semiconfined aquifer was selected in an industrial area at Vilafant (Alt Empordà, northeast Spain), about 150 km north of Barcelona. Two aquitards formed by fine sands and silts exist below the aquifer, where an aged source of PCE (i.e., an old free phase pool in which, after decades of groundwater flushing and dissolution, the DNAPL only partially occupies the pores at saturations below the residual saturation value (Puigserver et al., 2016a)) was detected in an immobile residual form. The shallower aquitard is of a continental character and the other is marine (ITGE, 1994).

2. Site description

2.1. History of the site

The site comprises a semiconfined aquifer made up of Pliocene materials. Chloroethene contamination was detected in 1980, but it is not known when it originated. The main contaminant is PCE, which was used as a degreaser of vehicle parts at a nearby industrial plant dedicated to the automotive industry. The PCE-DNAPL was probably dumped inside an old abandoned agricultural dug well located in the plant. Apart from the monitored natural attenuation, other remediation measures have not been implemented by the Catalan Water Agency (ACA). Groundwater contamination has resulted in concentrations of PCE that were still high in 2017 (up to 8.00 mg/L). Furthermore, the widespread use of manure as a fertilizer has led to diffuse nitrate pollution in the aquifers of the region.

The monitoring network consists of 12 conventional piezometers installed by the ACA. Detailed stratigraphic logs and geometrical characteristics of boreholes for these piezometers were facilitated by the ACA. Two of these piezometers (S4 and S12, Figs. 1 and 2) were screened in the deepest geological materials of a Pliocene marine lower aquitard constituted by fine sands and silts that between the depths of 25 and 30 m contain intercalations of conductive thin layers of medium sands

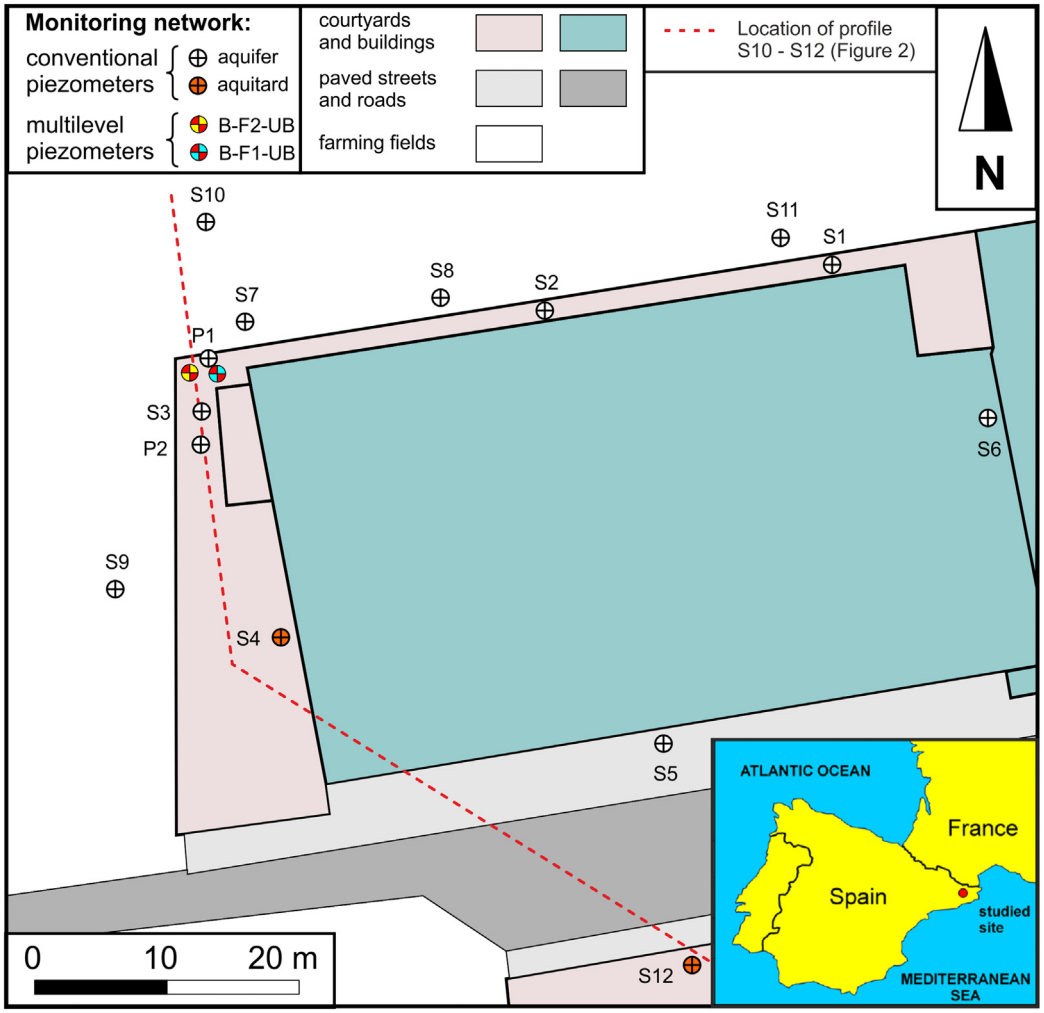

Fig. 1. Situation map of the contaminated site and monitoring network.

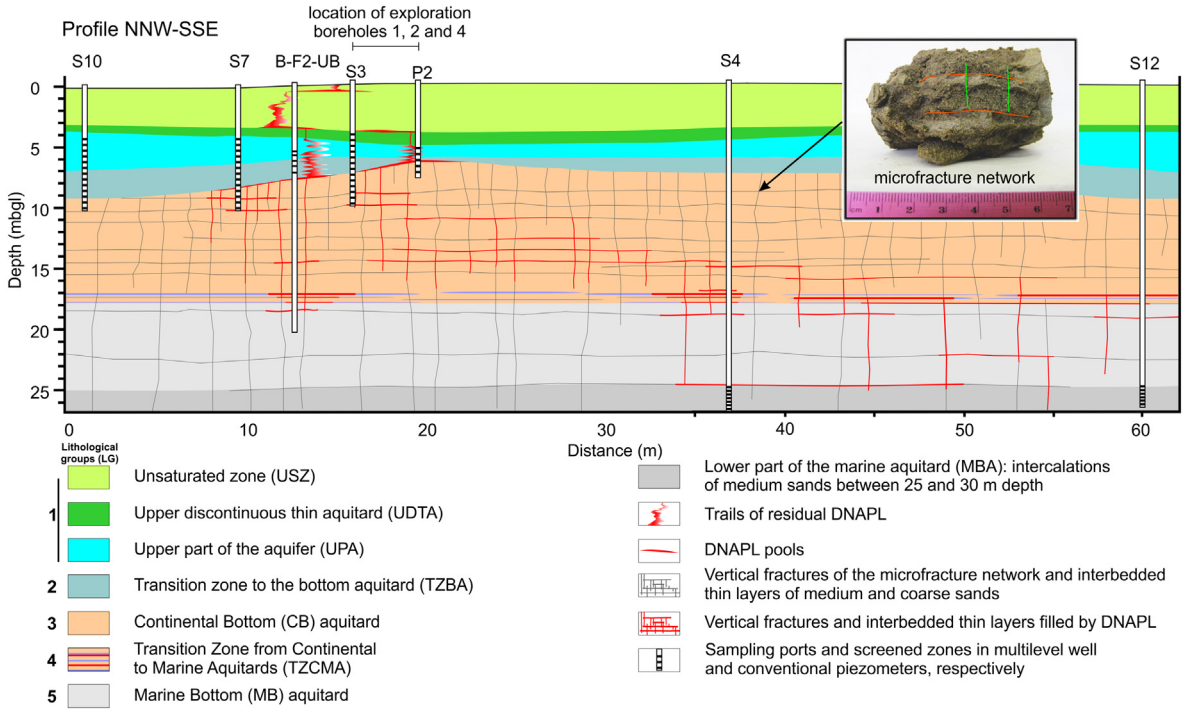

Fig. 2. Distribution profile of the hydrostratigraphic units at the site. S12, S4, P2, 1, 2 and 4, S3, B-F2-UB, and S10 are the drilled boreholes. The boreholes for the conventional piezometers are: S10, S7, S3, S4, and S12. The borehole for the multilevel well F2UB is B-F2-UB. The exploration boreholes are 1, 2, and 3. The borehole for a well is P2.

(Table 1 shows the geometrical characteristics of these piezometers). In addition, our Environmental Hydrogeology Research Group of the University of Barcelona (UB) drilled two boreholes (B-F1-UB and B-F2-UB) in January 2011 (Fig. 1) and constructed two screened wells (P1 and P2) in July 2017, in the aquifer and transition zone to a Pliocene continental lower aquitard.

2.2. Geological and hydrogeological framework

Subsurface materials correspond to Pliocene prograding alluvial fan deposits (ITGE, 1994; IGC, 1996) that are divided into five lithological groups. The shallowest part of the first group (with an average thickness of 5.8 m) is dominated by proximal deposits of gravels and sands that are mostly channelized and display high porosity. This part of the group forms the Unsaturated Zone (USZ in Fig. 2), under which some isolated discontinuous levels of clays and sands that form the middle part of this lithological group (1.2 m average thickness) constitutes the first hydrostratigraphic unit (the Upper Discontinuous Thin Aquitard [UDTA] in Fig. 2). This is followed by the third part of the group that is also composed of proximal deposits of channelized gravels and sands with high porosity (thickness between 1.5 and 4 m); it forms the Upper Part of the Aquifer (UPA in Fig. 2), which is the second hydrostratigraphic unit.

Below the first lithological group, deposits of distal alluvial fans (sheet-floods) made up of layers of gravels and sands interbedded with fine sands (Fig. 3) that are rich in organic matter form the second lithological group (with thicknesses ranging from 0.5 to 2.5 m) and constitutes the third hydrostratigraphic unit, the Transition Zone to the Bottom Aquitard (TZBA in Fig. 2). The TZBA is followed by the third lithological group, which corresponds to basin plain deposits that are mainly composed of fine sands and silts (Fig. 3) of a continental character with thicknesses between 8 and 10 m. Next is the fourth hydrostratigraphic unit, the Continental Bottom (CB) aquitard, formed by fine sands and silts (Fig. 2). The fourth lithological group follows; it is formed by fine sands interbedded with silts and gravels (Fig. 3). This group is relatively thin (only 0.8 m) and constitutes the fifth hydrostratigraphic unit, the Transition Zone between the Continental and Marine Aquitards (TZCMA). The fifth lithological group has a marine character and is formed by fine sands and silts, constituting another aquitard whose thickness is at least 10.2 m, and between 25 and 30 m deep, where it contains intercalations of medium sands (Figs. 2 and 3). This aquitard constitutes the sixth hydrostratigraphic unit, the Marine Bottom (MB) aquitard (Fig. 2).

Boreholes B-F1-UB and B-F2-UB and some conventional piezometers of the monitoring network reach the depth of the CB-aquitard. The stratigraphic correlation of logs of boreholes of the monitoring network showed that these units dip slightly to the northeast.

The aquifer is composed of two parts: i) one part of the proximal coarse-grained alluvial fan deposits (the UPA unit), in which hydraulic conductivities oscillate between 1.16×10^{-4} and 2.31×10^{-4} m/s, and ii) the distal alluvial fan deposits (the TZBA unit), whose hydraulic conductivities range between 1.16×10^{-5} and 1.16×10^{-4} m/s. Gravel paleochannels of the distal alluvial fan deposits in the UPA act as drainage lines, coinciding with the general flow toward the northeast, as

Table 1
Main characteristics of the piezometers screened in the Pliocene marine lower aquitard.

Piezometer	Total depth (m)	Depth range of screened zone (m)	Diameter of the borehole (mm)	Diameter of intubation (mm)	Depths range of bentonite (m)	Depths range of gravel filter
S4	30	25–30	65	55	0–24	24–30
S12	30	25–30	70	60	0–24	24–30

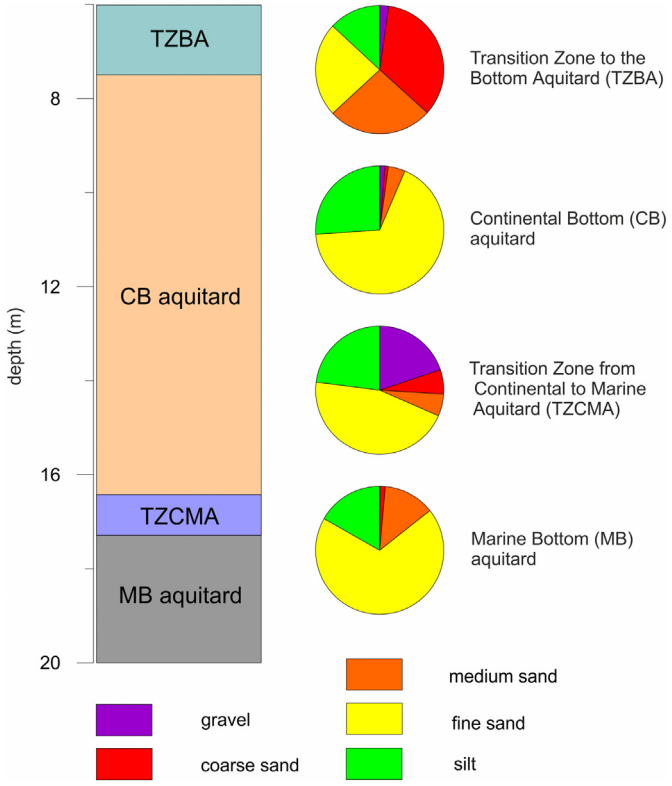

Fig. 3. Distribution profile of the hydrostratigraphic units in B-F1-UB and B-F2-UB with average grain sizes. Only borehole B-F2-UB reached the depths of the hydrostratigraphic units [TZCMA and MB-aquitard].

shown in Fig. 1. The average oscillation of the piezometric level during the year is 1.5 m, and the average gradient is 0.041. The fine sands and silts composing the two aquitards underlying the TZBA (CB-aquitard and MB-aquitard) are crossed by subvertical microfractures and horizontal bedding planes (Puigserver et al., 2016a).

3. Materials and methods

3.1. Procedures to test the working hypotheses

The two working hypotheses established are related to the identification of the zones where reactive abiotic and biotic reductive dichlorination are favored. To test these hypotheses, a hydrostratigraphic analysis of continuous cores from the site was conducted. For this purpose, two boreholes were drilled at the source. The detailed description of these boreholes made it possible to differentiate the six hydrostratigraphic units mentioned in Section 2.2, three of which constituted aquitards. Of these hydrostratigraphic units, the three below the TZBA (Fig. 2)—two aquitards (CB and MB) and the transition zone between them (TZCMA)—were studied in this work (see Section 2.2). Furthermore, the porewater and sediments of aquitards and the transition zone of these three units (Fig. 2) were analyzed to characterize them chemically. Groundwater in the interlayered levels of medium sands of conventional piezometers S4 and S12 (see Section 2.1) was also analyzed. Section 3.2 indicates the analyzed compounds. The purposes of these analyses were diverse: to gain insight into how PCE-DNAPL distributes in microfractures, bedding planes, and interstratified conductive layers, as well as the maturity degree of this DNAPL; to determine how dissolved PCE and other chloroethenes distribute in the matrix to identify the biogeochemical processes involved; to evaluate where in the aquitard most biogenic activity occurs; and to detect the depths where the highest degradation of chloroethenes develops.

3.2. Borehole drilling, sampling, and chemical determinations

3.2.1. Borehole drilling

Boreholes B-F1-UB and B-F2-UB were created by rotary drilling with a diamond crown bit, with a provisional metal sleeve casing with an external diameter of 127 mm. A core-sampler (85 mm internal diameter) was used to recover the core. The drilling operations and the core-sampler have been described by Puigserver et al. (2016a).

3.2.2. Core sampling, conservation protocols, and analytical determinations

The cores are described in detail in Fig. 2. They were exhaustively sampled to characterize the vertical distribution of concentrations of PCE, TCE, cDCE as well as *trans*-dichloroethene (tDCE), 1,1-dichloroethene (1,1-DCE), and VC in the porewater of aquitards. Chloroethene concentrations were determined at the Scientific and Technological Centers of the University of Barcelona (STC-UB). A total of 71 core sediment samples were taken at B-F1-UB and B-F2-UB to analyze chloroethene concentrations. The sampling of cores also served to obtain the isotopic composition of these compounds in porewater. The ^{13}C isotopic composition of chloroethenes retained in the porous matrix adjacent to the aquitard microfractures was analyzed. The compound-specific isotope analysis (CSIA) approach was used for these determinations. Given the low concentrations of cDCE (concentrations of the other DCE isomers were even lower) and VC, only the isotopic composition of PCE and TCE could be assessed. CSIA determination was carried out at the STC-UB. The purpose of these determinations was twofold: i) to determine the degree of biotic or abiotic degradation occurring within the matrix, and ii) to analyze the role in chloroethene degradation of sessile microorganisms in the aquitard porewater compared with that of benthic microorganisms that move with the groundwater flow. Sediment cores were also sampled to analyze the total Fe and Mn (as sorbed or solid phase of Fe and Mn) in the fine clay fraction of sediments in the aquitards (obtained from the aliquots of *aqua regia* extractions). Analyses were performed at the STC-UB. This fine fraction was also analyzed using scanning electron microscopy (SEM) at the STC-UB to determine to which minerals the measured Fe corresponded. The percentage of organic carbon (f_{oc}, a parameter that is directly related to the amount of organic matter in the medium) and the microbial communities in these sediments were also determined at the STC-UB. In both cases, the sampling procedures have been described by Puigserver et al. (2013). Core sampling was performed taking into account lithological changes, textural changes, and microfractures following the criteria indicated by Guilbeault et al. (2005) and Parker et al. (2008).

Special emphasis was placed on the microfracture zones (inside the microfractures and in the surrounding matrix), in the textural changes in the aquitards, in the intersection (joint-points) of microfractures with, in general, any type of subhorizontal bedding planes, and where alteration aureoles were observed.

A total of 80 core sediment samples were taken at B-F1-UB and B-F2-UB for f_{oc}, Fe and Mn. The sampling for chloroethenes consisted of obtaining: i) 15 core samples from the TZBA (6 samples from B-F1-UB and 9 samples from B-F2-UB), ii) 45 core samples from the CB-aquitard (27 samples from B-F1-UB and 18 samples from B-F2-UB), and iii) 4 core samples from the TZCMA and 7 from the MB-aquitard (in both cases only from B-F2-UB, as B-F1-UB did not reach the depth of these hydrostratigraphic units). All the samples for chloroethene concentrations and their isotopic compositions ($\delta^{13}C$) were taken in triplicate, and the other analyses were performed in duplicate. Likewise, field, transport, reactant, and instrumentation blanks were taken for every 20th field sample. Samples for molecular analysis were collected in sterilized vases and frozen in the field. To prevent cross-contamination during the entire sampling process, the material used was cleaned with soapy water, methanol, and distilled water between consecutive samples.

Sampling procedures and conservation protocols as well as the calculations of the porewater concentrations of chloroethenes were an

adaptation of those followed by Chapman and Parker (2005) for granular media. To minimize volatilizations, a methanol trap (methanol, Merck, ISO Pro analysis) was used in accordance with EPA SW-846, Method 5035. In the case of the samples destined for the determination of the isotopic composition of $\delta^{13}C$ of chloroethenes in porewater of the matrix of fine sediments, the dimethylacetamide (DMA) trap method developed by Herrero et al. (2021a) was used. Sediment samples from cores were also taken to determine the dry and wet bulk densities and porosities to calculate the chloroethene concentrations in the porewater (Chapman and Parker, 2005). The samples collected for the analysis of Fe, Mn, and f_{oc} were frozen on site and stored at −20 °C.

Sudan IV screening for colorimetric determination of the DNAPL free or residual phase was conducted during the drilling of the two boreholes following the method described by Hartog et al. (2010).

Molecular analyses were carried out at the Helmholtz Centre for Environmental Research – UFZ (Leipzig, Germany). DNA was extracted with the NucleoSpin® Soil kit (Macherey–Nagel) following the manufacturer's protocol.

3.2.3. Groundwater sampling and conservation protocols

Groundwater from S4 and S12 were sampled to analyze PCE, TCE, cDCE, tDCE, 1,1-DCE, VC, and $\delta^{13}C$ of chloroethenes, as well as nitrate, nitrite, sulfate, Fe, and Mn. DO, the redox potential (Eh), pH, and electrical conductivity (EC) of groundwater were measured on site in these conventional piezometers. Sampling, transport, and storage protocols have been described by Puigserver et al. (2016a).

3.3. Sample pretreatments and analytical techniques

Core sampling and extraction of chloroethenes (sorbed and dissolved in porewater) was conducted in the laboratory following the guidelines reported by Puigserver et al. (2013, 2016a, 2016b), which were an adaptation of the protocol described by Dincutoiu et al. (2003). Gas chromatography–mass spectrometry (GC–MS) was used to determine chloroethene concentrations in the core samples. Core samples to determine $\delta^{13}C$ values of chloroethenes in the porewater were pretreated according to the protocols described by Herrero et al. (2021a) and analyzed by gas chromatography–isotope ratio mass spectrometry (GC-IRMS) with solid phase microextraction (SPME).

The sampling and pretreatment protocols to determine f_{oc}, and sorbed or solid phase of Fe and Mn in core soil sediments, as well as the corresponding analyses were the same as those described by Puigserver et al. (2013, 2016a, 2016b). The determination of f_{oc} was performed by elemental analysis using the gas chromatography technique with a thermal conductivity detector (TCD). The analyses of Fe and Mn were conducted by inductively coupled plasma optical emission spectroscopy (ICP-OES).

The Fe oxide mineral precipitates between clay minerals were identified by the Scanning Electron Microscopy technique (SEM).

Groundwater was sampled as described by Puigserver et al. (2016a) and analyzed by the GC–MS and GC-IRMS with SPME techniques to determine chloroethene concentrations and $\delta^{13}C$ values, respectively. Nitrate, nitrite, and sulfate in groundwater were analyzed by ion chromatography. The analyses of Fe and Mn dissolved in groundwater were conducted by the ICP-OES technique.

To determine the richness of bacterial communities, and the presence of *Dehalococcoides* and *Propionibacterium acnes*, sediment core samples taken and immediately frozen at the field site at −20 °C were used. Genomic DNA was extracted from these samples according to Puigserver et al. (2016a, 2016b) and polymerase chain reaction (PCR) was performed. For the detection of *Dehalococcoides*, primers 582f (CTG TTG GAC TAG AGT AGT ACA GC) (Duhamel et al., 2004) and 728r (GTG ACA ACC TAG AAA ACC GCC TT) (Löffler et al., 2000) were used utilizing the PCR conditions described by Löffler et al. (2000). For the detection of vcrA (vcrA f CTA TGA AGG CCC TCC AGA TGC and vcrA rGTA ACA GCC CCA ATA TGC AAG TA) (Holmes et al., 2006) and bvcA (bvcA f TGC CTC AAG TAC AGG AGG TGG T and bvcA r ATT GTG GAG GAG GAC CTA CTA CCT) (Krajmalnik-Brown et al., 2004), PCR was performed following the conditions described in the Supporting Information (SI) document.

The microbial richness and the presence of *P. acnes* were assessed by T-RFLP analysis of the 16S rRNA gene according to Herrero et al. (2021b). Two sediment samples were chosen in the TZBA to conduct clone library analyses to distinguish the microbial communities from the pool and just above it, to identify the restriction fragments from T-RFLP; and thus, corroborate that these communities may locally contain different bacteria involved in reductive dechlorination.

More detailed information is provided on the methods section of the SI document.

4. Results and discussion

4.1. Control over the distribution of the PCE-DNAPL primary source exerted by the geologic contact surface between the TZBA-unit and the CB-aquitard

The detailed geological description of the first and second lithological groups (from the USZ to the TZBA, see Section 2.2 and Fig. 2) was carried out from research surveys during drilling B-F1-UB and B-F2-UB and has been reported by Puigserver et al. (2016a).

PCE-DNAPL spills from the upper levels accumulated on the geologic contact surface between the TZBA and the CB-aquitard soon after the contamination episode. These accumulations formed some PCE-DNAPL pools that constituted the primary source of the PCE-DNAPL at this site. They are currently divided into portions, some of which are still in a continuous free phase and others that have reached a mature stage (aged pools; Mercer et al., 2010).

The mentioned geological surface contact was located at a depth of 6–9.2 m (Fig. 2), 19 and 22 m above sea level. This contact corresponded to a paleo-relief produced by the erosive incision of paleochannels of the upper units. In the area of S12 (Fig. 2), this contact was located at a greater depth than in the area of P2 (which coincided with a well-defined inter-channel zone), while in the area of S10, the contact was also located at a greater depth than in P2. The orientation of these paleochannels was from southwest to northeast, conditioning the general groundwater flow of the system toward the northeast, as described by Puigserver et al. (2016a). This paleochannel structure also conditioned the migration of the DNAPL in the free phase at the primary source. Thus, in P2, where the geological contact was deeper, the aforementioned inter-channel zone constituted a division in terms of DNAPL migration through this contact. Thus, the DNAPL discharged north of P2 migrated northward, while the DNAPL discharged south of P2 migrated southward (i.e., against the main groundwater flow direction, which follows the main dipping direction of the thalweg line of the paleochannel).

4.2. Hydrostratigraphic characteristics of the studied aquitards

For the fine sands and silts (Fig. 3) of the CB-aquitard, 68% of sands were a silty-clay matrix (Fig. 3); they were accompanied by interstratified silt levels (silts represented approximately 26%). This aquitard was also crossed by numerous subvertical microfractures that, in connection with bedding planes and thin layers of coarser sands and representing textural contrasts with the fine sands, gave rise to an orthogonal network (see photograph in Fig. 2). This network favored vertical (Fjordbøge et al., 2017) and horizontal migration of the PCE-DNAPL along these discontinuities, which became secondary sources of the PCE-DNAPL. This aquitard corresponded to materials of a continental origin and showed a high degree of compaction, which accounted for their low K values (from 1.16×10^{-7} to 1.04×10^{-5} m/s). Despite this low range, the K values were fairly homogeneous throughout the aquitard, although the increase in lithostatic pressure with depth favored a decrease in K of fine sands up to 17.2 m, where the bottom of this aquitard

was located. The hydrostratigraphic unit corresponding to the TZCMA (Fig. 2) was found at this depth. There, interstratified layers with compacted fine sands similar to those of the previous unit, and thin layers of fine gravels to medium sands with a silty-clayey matrix began to occur (Fig. 5). Gravel comprised 51% of this unit (Fig. 5), and the percentage of fine sand (24%) was decreased. These changes imply an increase in K values (with values ranging from 1.16×10^{-4} to 1.85×10^{-4} m/s), enabling groundwater flow throughout this unit. This unit reached a depth of 18.3 m when the deepest aquitard, that of marine origin (MB-aquitard), was found (Fig. 2).

In this new unit, from a depth of 20 m in the borehole of piezometer S4 and 24 m in S12, there was an increase in interstratified layers containing bivalve fragments. The color of this marine aquitard was much darker, coinciding with an increase in organic matter content, with f_{oc} values of up to 0.048%, higher than those of the aquitard of continental origin (with an average value of 0.0285%; see Section 4.3). The presence of numerous intercalated thin layers of more permeable materials, medium sands between fine sands (see Section 2.2), allowed groundwater flow throughout this unit.

4.3. Distribution of Fe, Mn, and f_{oc} in sediments of the lower continental and marine aquitards

Fig. 4 shows the low variability in f_{oc} percentages in sediments within the CB-aquitard. Nevertheless, the f_{oc} percentages in this aquitard (with average values of 0.029% and 0.028% in B-F1-UB and B-F2-UB, respectively) were considerably higher than those recorded in the TZBA, especially at the depth where there was greater degradation of the accumulated PCE-DNAPL, namely B-F1-UB (Puigserver et al., 2016a), with an average value of 0.008%. On the other hand, among the minima in Fig. 4a, the minimum corresponding to label $2f_{oc1}$ (0.025%) stands out: It coincided with the depth where minimum PCE (below the LOQ) and maximum TCE (Fig. 6a, label $1TCE_1$, with 7.2 μmol/L) were recorded. Regarding the MB-aquitard, the maximum f_{oc} percentages recorded at the upper part of this hydrostratigraphic unit, with a peak of 0.037% (Fig. 4a, label $2f_{oc2}$), coincided with a peak in the concentration of TCE (Fig. 6b, label $2TCE_1$, 3.5 μmol/L) and with the presence of fine to medium interstratified gravel levels.

Regarding Fe and Mn, peaks of these metals in the lowest part of the TZBA were registered at B-F1-UB (Fig. 4a and b, labels $1Fe_1$ and $1Mn_1$; 667 μmol/g of Fe and 34 μmol/g of Mn, respectively). In the case of the CB-aquitard, two sampling points at a depth immediately below the mentioned peaks in the TZBA continued recording high Fe and Mn values (286.5 and 220.8 μmol/g for Fe and 20.2 and 20.1 μmol/g for Mn; Fig. 4a and b). These concentrations were higher than that of the average values in the rest of this continental aquitard in B-F1-UB (194.4 and 16.4 μmol/g of Fe and Mn, respectively). The high Fe and Mn values of these two sampling points coincided with high concentrations of PCE at the uppermost part of the CB-aquitard below peaks of PCE in the lower part of the TZBA (Fig. 6a and b, labels $1PCE_1$ and $2PCE_1$, 102 and 9.2 μmol/L, respectively). The fine clay fraction was analyzed using SEM, and mineral precipitates of Fe oxides and Mn oxides were identified accompanying the clay minerals.

Below the aforementioned high Fe values in the uppermost part of the CB-aquitard at B-F1-UB (286.5 and 220.8 μmol/g; Fig. 4b), Fe concentrations were high (194.4 μmol/g in average) compared with the uppermost part of the TZBA (Puigserver et al., 2016a), where 117.9 μmol/g of Fe was recorded. A peak of Fe (298 μmol/g; Fig. 4b, label $2Fe_1$) was recorded at the bottom of the TZCMA, coinciding with the presence of interstratified layers of fine gravels and with an increase in concentrations of PCE and TCE (Fig. 6b, labels $2PCE_2$ and $2TCE_1$, 0.52 and 3.5 μmol/L, respectively). This is again a similar scenario to that described earlier for the case between the TZBA and the CB-aquitard and suggests sufficient reducing conditions to result in PCE degradation and to favor the formation of Fe oxide mineral precipitates that occur with the clay minerals (He et al., 2015), which have been identified with SEM. The maximum Fe concentration (Fig. 4b, label $2Fe_2$, 318 μmol/g) also coincided, as mentioned previously, with the increase in TCE (Fig. 6b, label $2TCE_2$, 13.3 μmol/L), which was not accompanied by an increase in either cDCE or VC. These findings suggest that TCE is proportionally less degraded and/or that the degradation products correspond to an abiotic (Schaefer et al., 2018) rather than a microbial degradation. According to He et al. (2015), the identified iron oxides and clay minerals could contain sorbed Fe^{2+} ions. The same authors stated that these minerals promote abiotic degradation processes of chloroethenes.

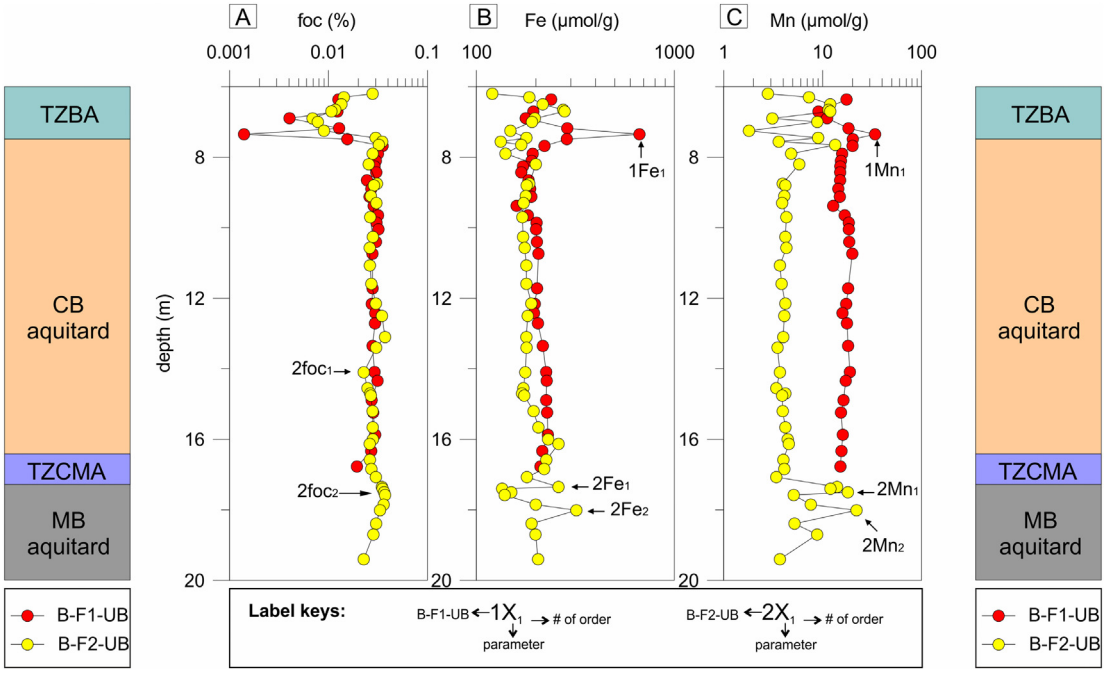

Fig. 4. Variation in Fe, Mn, and f_{oc} concentrations with depth in the hydrostratigraphic units.

Regarding Mn, a peak (17 μmol/g; Fig. 4c, label $2Mn_1$) was located at a slightly greater depth than the $2Fe_1$ peak. Moreover, this Mn maximum occurred at a depth where cDCE concentrations were decreasing (such a decline commenced from the cDCE peak corresponding to the $2cDCE_1$ label (Fig. 6b, 0.092 μmol/L)). This finding could indicate that the maximum production of cDCE occurs under redox conditions that are even more reducing than Fe-reducing conditions (i.e., under sulfate-reducing conditions), when the formation of Fe oxide mineral precipitates has already been produced (Guilbaud et al., 2013). The $2Fe_2$ peak (Fig. 4c, 318 μmol/g) is attributable to abiotic degradation of chloroethenes and coincides with label $2Mn_2$ (20.03 mol/g).

4.4. Percentage of quantifiable PCE and TCE concentrations in the porewater

Table 2 summarizes some statistical measures of dispersion and centralization of the data. The dispersion measures are the range and the ratio of the standard deviation of the arithmetic mean (i.e., the coefficient of variation). As a centralization measure, the table contains the values of the arithmetic mean. These measures provide an overview of the statistical distribution for the population samples composed of the PCE and TCE concentration data in the porewater of the fine sediments in the two boreholes B-F1-UB and B-F2-UB drilled in the hydrostratigraphic units studied. Table 2 shows the percentage of samples in which PCE or TCE was measured (i.e., those samples in which their concentrations in the porewater of the fine sediments could be quantified and was therefore above the limit of quantification [LOQ]). The hydrostratigraphic units studied were (Fig. 2): 1) the Transition Zone to the Bottom Aquitard (TZBA), 2) the Continental Bottom aquitard (CB-aquitard), 3) the Transition Zone between the Continental and Marine Aquitards (TZCMA); and 4) the Marine Bottom aquitard (MB-aquitard).

Table 2
Summary of statistical measures of dispersion and centralization of PCE and TCE concentration data in the aquitards and transition zones. % ALOQ indicates the percentage of samples whose concentrations are above the limit of quantification. The arithmetic mean (AM) and coefficient of variation (CV) of the concentration values ALOQ are shown.

		B-F1-UB		B-F2-UB	
		PCE (mol/L)	TCE (mol/L)	PCE (mol/L)	TCE (mol/L)
For the whole TZBA. CB. TZCMA and MB units	Max	112.88	10.08	8.87	15.02
	Min	0.04	0.03	0.06	0.05
	AM	11.81	1.74	1.61	1.53
	CV	2.19	1.57	1.46	1.90
	% ALOQ	69.70	58.97	64.86	68.42
TZBA	Max	13.01	10.08	8.87	8.25
	Min	0.16	0.03	0.06	0.06
	AM	3.71	4.65	1.41	0.90
	CV	1.68	0.86	2.03	2.88
	% ALOQ	83.33	100.00	100.00	62.50
CB aquitard	Max	112.88	1.56	6.36	2.70
	Min	0.04	0.04	0.06	0.06
	AM	13.52	0.62	2.69	0.62
	CV	2.08	0.86	0.82	1.56
	% ALOQ	71.43	46.43	61.11	75.00
TZCMA	Max	–	–	0.13	3.36
	Min	–	–	0.06	1.52
	AM	–	–	0.10	2.64
	CV	–	–	0.47	0.28
	% ALOQ	–	–	50.00	100.00
MB aquitard	Max	–	–	0.55	15.02
	Min	–	–	0.16	0.05
	AM	–	–	0.37	4.41
	CV	–	–	0.49	1.38
	% ALOQ	–	–	57.14	60.00

(−) Borehole B-F1-UB did not reach the depth of this unit.

In the case of PCE, for all of the studied units, the highest percentage of samples whose concentrations were above the limit of quantification (% ALOQ), and therefore could be quantified, was recorded in B-F1-UB (Table 2), together with a higher average molar concentration of PCE than in B-F2-UB. This higher concentration in B-F1-UB is in agreement with the higher concentration recorded in the TZBA (where the primary source of the PCE-DNAPL was located; see Section 4.1), and in the CB-aquitard of this borehole (where secondary sources of PCE-DNAPL from TZBA leaks were located; see Section 4.2). Although borehole B-F1-UB did not reach the depths of the TZCMA, the presence of PCE in this unit in B-F2-UB, and even more concentrated at greater depths in the MB-aquitard, shows that the PCE-DNAPL of the primary source gave rise to secondary sources at the depths of these two hydrostratigraphic units in the area of B-F2-UB (see Section 4.2).

Regarding TCE for all of the units studied, the highest % ALOQ was observed in B-F2-UB. Although the concentration of the parent PCE in B-F1-UB was much higher than in B-F2-UB, the average molar concentration of TCE in B-F1-UB was only slightly higher than in B-F2-UB. These TCE concentrations coincided with high values of cDCE and VC in the latter borehole (not shown in Table 2), which is evidence of a greater degradation of PCE to TCE (and to cDCE and VC) in B-F2-UB (see Section 4.5.2). Other isomers of DCE (tDCE and 1,1-DCE) were not detected in either of the boreholes.

4.5. Geological heterogeneities controlling the distribution of PCE-DNAPL secondary sources in the aquitards

Apart from reactive abiotic and biotic degradation, sorption, molecular diffusion, and other fate processes, the variability in chloroethene concentrations in the porewater (Fig. 5) is also a consequence of the structure of the aquitards and the PCE-DNAPL distribution. The main factor controlling the migration of the PCE-DNAPL free phase is the microfracture network of the aquitard. Thus, Fig. 5 shows how, when the current PCE aged pool located at the TZBA was still a free phase pool and at a young stage of evolution (i.e., before 1980 when the contamination was detected; see Section 2.1), it had migrated by gravity through the subvertical microfracture network in the CB-aquitard (similarly to the phenomenon described by Rezaei et al. (2013) that crosses the fine sands with a silty matrix of the aquitard. In addition, there are stratification patterns marked by the existence of subhorizontal textural contrasts (see photograph in Fig. 2) at different depths in the aquitards. These contrasts correspond with more competent layers of fine-medium sands with a higher silt content that present greater compaction than fine sands (Fawad et al., 2010). These more competent layers define subhorizontal bedding planes, which allow the lateral migration of the PCE free phase by capillary forces (see Section 1) at different depths (Dearden et al., 2013).

In the joint-point zones, where subvertical microfractures intersected with bedding planes, PCE concentrations in the porewater were higher (Fig. 5, labels $1PCE_2$ and $1PCE_3$, 11.1 and 32 μmol/L). The microfracture network and bedding planes formed an orthogonal system of discontinuities with a space between microfractures and bedding planes of up to 1.5 cm × 1 cm, with microfracture openings of around 0.5–1 mm. This structure favors a rapid migration of the PCE-DNAPL free phase because the smaller the microfracture openings, the greater the capacity for a rapid migration of the PCE-DNAPL free phase by capillary action (Fjordbøge et al., 2017). This resulted in a significant and rapid dispersion of the DNAPL, which was followed by molecular diffusion of PCE into the matrix adjacent to the microfractures, bedding planes (Yang et al., 2012), and interstratified conductive layers due to significant textural changes in sediments. This phenomenon accounts for the presence of PCE in the porewater (Fig. 5) as a consequence of the accumulation of this contaminant in the matrix. Fig. 5 shows the vertical distribution of the main textures in the aquitards and their relationship with the PCE distribution in the porewater.

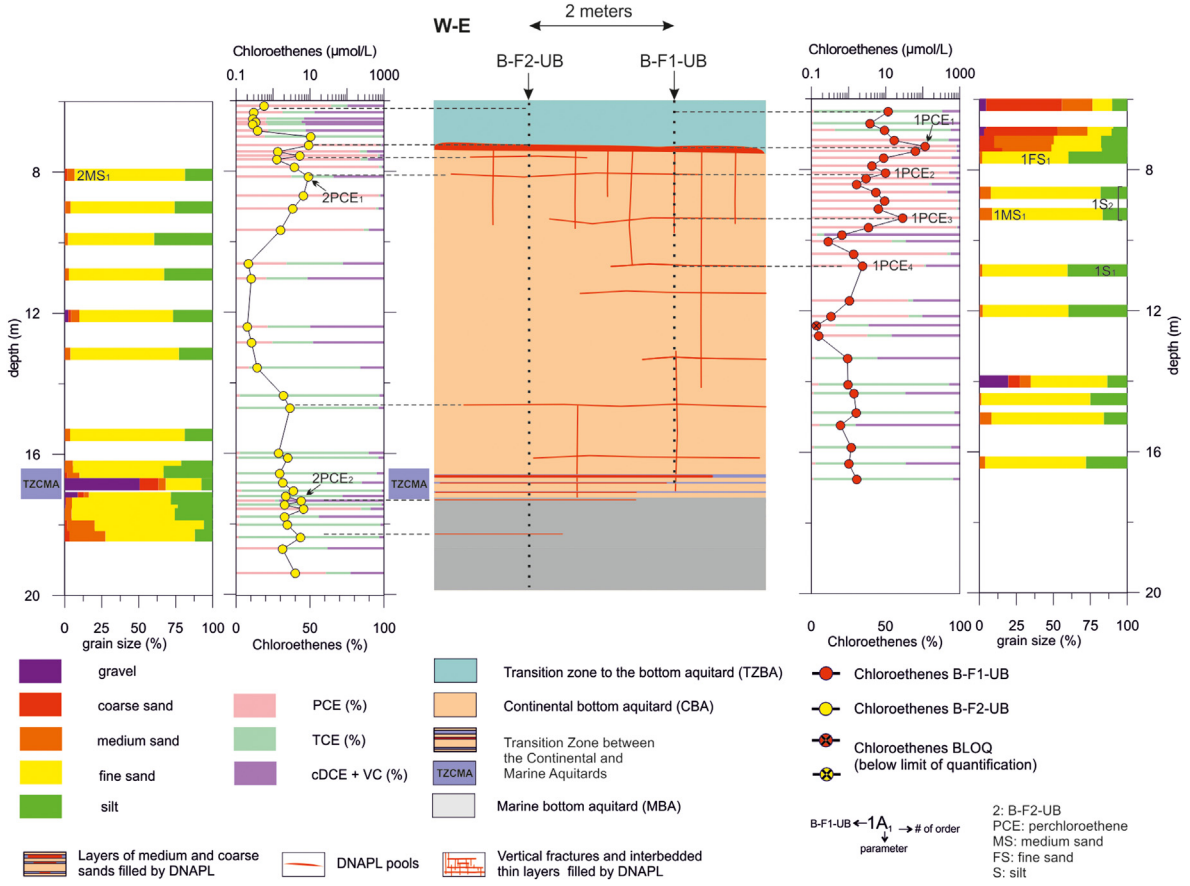

Fig. 5. Distribution of PCE concentrations as a function of depth textural changes.

In the TZBA, there are portions of the primary source pool in which the PCE-DNAPL is already in a residual aged state after decades of groundwater flushing. This means that the DNAPL only partially occupies the pores at saturations below the residual saturation value (Hartog et al., 2010) and constitutes an immobile phase formed by discontinuous nodules retained by capillary forces (Cohen and Mercer, 1993). However, there are still parts in which the PCE-DNAPL is found as a free phase connected to the network formed by the microfractures, interstratifications of conductive levels, and bedding planes. This finding implies that the primary PCE source is capable of continuing to allow the migration of the PCE free phase through the microfracture network because the PCE that penetrates by molecular diffusion into the matrix (as shown in Fig. 5; Lu et al., 2014) has completely degraded.

Fig. 5 shows how the important changes in granular textures in the TZBA have favored in the past the accumulation of pools of the PCE-DNAPL free phase. These pools are now practically all in a residual form (aged pools; Fig. 5, label $1PCE_1$, 102 µmol/L) in an equivalent way as described by Rivett et al. (2014). This is a depth where the proportion of fine sands and silts increased significantly (Fig. 5, label $1FS_1$). To a lesser extent, this was also observed in a deeper zone (Fig. 5, label $1PCE_4$, with a PCE concentration of 1.7 µmol/L, and label $1S_1$), where the substantial increase in silts relative to fine sands has favored the accumulation of the PCE-DNAPL that migrated by gravity-capillary action through the aquitard.

At shallower depths, dots identified with labels $1PCE_3$ and $2PCE_1$ in Fig. 5 (32 and 9.2 µmol/L, respectively) show that PCE contents were related to a decrease in the percentage of silts and an increase in medium sands (Fig. 5, labels $1MS_1$ and $2MS_1$). This relationship is linked to the fact that at depths where the proportion of silt is lower, the percentage of PCE that migrates by molecular diffusion decreases. Consequently, the maxima of PCE concentrations are caused by the migration of this compound as a free phase.

The increase in PCE concentrations in the porewater in the interstratified layers of fine gravel with silty matrix at the bottom of the TZCMA (Fig. 5, label $2PCE_2$, 0.52 µmol/L) confirms that migration of the PCE free phase through the subvertical microfractures has led to: i) the accumulation of the PCE-DNAPL at depths where significant contrasts in K occur, and ii) the lateral movement of the PCE free phase above the less permeable layers (Luciano et al., 2010; Puigserver et al., 2020), which accounts for the fact that at these depths, the PCE concentration is much higher than in the upper depths of the CB-aquitard. In addition, the fact that PCE-DNAPL accumulations still exist as the residual phase at the depths of the TZCMA accounts for the fact that at greater depths, the presence of dissolved PCE in groundwater is still detected (i.e., those depths at which conventional piezometers S4 and S12 are open).

4.5.1. Distribution of the parent PCE and isotopic composition in the aquitards

Fig. 6 shows the observed results of PCE concentration profiles at boreholes B-F1-UB and B-F2-UB. In general, there was a trend of decreasing concentrations with depth within the CB-aquitard. However, in the upper half portion of this aquitard, there were depths at which porewater concentrations were very high. In contrast, concentrations were much lower further down (and even, in the deeper zones, values below the LOQ were recorded). Very high concentrations of PCE stand out at different depths. This was the case of those recorded in the uppermost part of the CB-aquitard (labels $1PCE_1$ and $2PCE_1$, 102 and 9.2 µmol/L, respectively; Fig. 6a and b, respectively). In the joint-point zones, PCE concentrations in the porewater were also high (Fig. 6a, labels $1PCE_2$

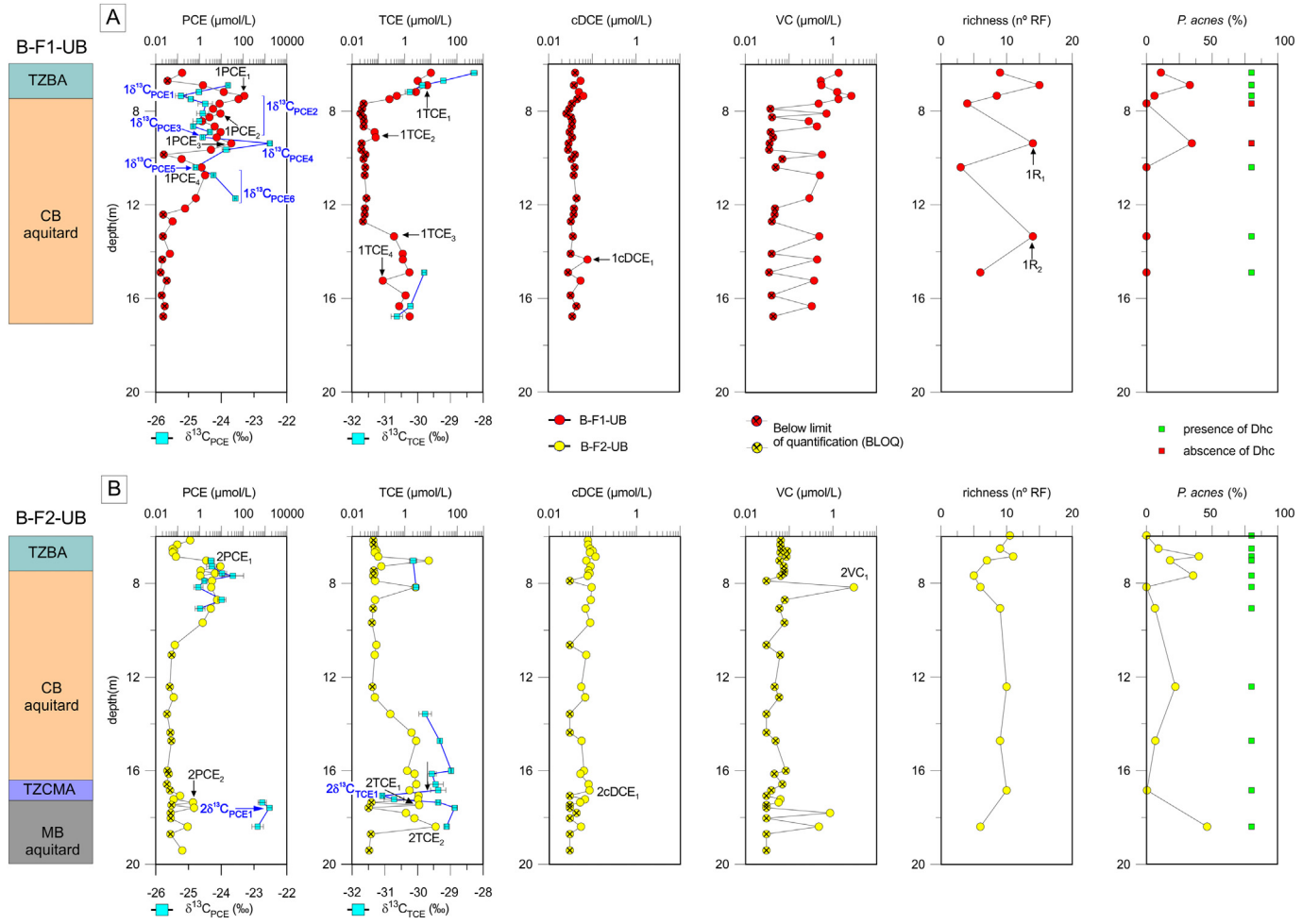

Fig. 6. Variation in the concentration and isotopic composition of chloroethenes and the microbial richness and presence or absence of *Dehalococcoides* (Dhc) spp. and *Propionibacterium acnes* (*P. acnes*) with depth.

and $1PCE_3$, 11.1 and 32 µmol/L, respectively). In addition, depths were textural contrasts between adjacent layers occurred, also high concentration were recorded (Fig. 6a, label $1PCE_4$, 1.7 µmol/L). At borehole B-F2-UB, near the base of the TZBA, high PCE concentrations were recorded at the depth where residual phase of PCE-DNAPL was found, with a maximum value in the sample labeled $2PCE_1$ (9.2 µmol/L). Moreover, at contact TZCMA and MB-aquitard, where interbedded layers of fine to medium gravels occurred high PCE concentrations were detected in B-F2-UB (Fig. 6b, label $2PCE_2$, 0.52 µmol/L).

Fig. 6 also shows the variation profile of $\delta^{13}C$ values of PCE in the porewater of the aquitards in the two boreholes. Although a tendency to less negative values was observed with depth, variations with minima of negative values and maxima of less negative values were recorded. Among these minima values, at borehole B-F1-UB, it is worth mentioning that recorded in the pool at the top of the CB-aquitard (Fig. 6a, label $1\delta^{13}C_{PCE1}$, −25.2‰ ± 0.5‰). Immediately below that pool, where a high percentage of silt was detected, less negative values were recorded (Fig. 6a), although reaching values close to −25‰ in the depth range labeled as $1\delta^{13}C_{PCE2}$. Below, at a depth where the percentage of fine sand increased, the $\delta^{13}C$ PCE values recorded were more negative (Fig. 6a, label $1\delta^{13}C_{PCE3}$, −24.6‰ ± 0.1‰). At a depth where an increase in silt coincided with a joint-point zone, the PCE recorded a less negative $\delta^{13}C$ value than at shallower depths (Fig. 6a, label $1\delta^{13}C_{PCE4}$, −22.6‰ ± 0.2‰). Deeper still, in a zone where textural contrasts between sediments were identified, the PCE recorded very negative $\delta^{13}C$ values (Fig. 6a, label $1\delta^{13}C_{PCE5}$, −24.8‰ ± 0.1‰). Below this zone, mainly between silts, the $\delta^{13}C$ values of the PCE measured became less negative, as indicated by the two dots on the depth range marked with the label $1\delta^{13}C_{PCE6}$ of Fig. 6a, whose least negative value was −23.51‰ ± 0.1‰. As regards the B-F2-UB borehole, the maximum $\delta^{13}C$ values of PCE (i.e., less negative) that were recorded in the MB-aquitard stand out, among which highlights that indicated with the label $2\delta^{13}C_{PCE1}$ (Fig. 6b, −22.5‰ ± 0.2‰).

The above results of PCE concentrations and $\delta^{13}C$ values are discussed below in the framework of the results presented and discussed in the previous sections. Fig. 5 shows that on the geological contact surface between the TZBA and the CB-aquitard, there is an aged pool of PCE that, from the early times of the contamination episode to the present time, has led to migration of PCE by molecular diffusion into the matrix of the CB-aquitard (see introduction of Section 4.5). The PCE isotopic composition of the pool was determined; it is denoted in Fig. 6a by the dot labeled $1\delta^{13}C_{PCE1}$, which corresponds to the value −25.2‰ ± 0.5‰ (the most negative $\delta^{13}C$ value of PCE). This is the closest value to the isotopic composition of the initially spilled PCE-DNAPL, when the PCE from the pool migrated into the porewater by molecular diffusion. Thus, more positive $\delta^{13}C$ values in PCE suggest that a reactive abiotic or biotic degradation process could have occurred. However, for these processes to be ascribed to the category of reactive processes, the mentioned shifts should be greater than 2‰, which is the threshold value reported by Wanner et al. (2017) that considers the effect of isotopic fractionation owing to molecular diffusion combined with that caused by sorption (see Section 1). Regarding biodegradation and abiotic degradation processes other than molecular diffusion or sorption, the shift

in PCE isotopic fractionation values in the CB-aquitard and MB-aquitard (Fig. 6) was 2.65‰. This value is higher than the mentioned threshold value, which suggests that PCE degradation is likely to have occurred.

As Puigserver et al. (2016a) have demonstrated, on the exterior surface of the pool there is a biofilm (denoted as biodegradation halo by these authors) that favors the degradation of PCE as it dissolves from that surface. The fact that the interface between the TZBA and the CB-aquitard is an ecotone (Puigserver et al., 2013; Herrero et al., 2021c) favors the degradation of the PCE-DNAPL pool. This causes PCE to change isotopically from being lighter in the internal part of the pool to heavier in the most external part of the pool. Hence, PCE constituting the DNAPL in that most external part of the pool is degraded, which in turn favors bioenhancement in the pool dissolution process. By contrast, below the pool (at the depth of the CB-aquitard, where a significant percentage of silt was detected; Fig. 5, label $1S_2$) PCE degradation occurred (Fig. 6a, in depth range labeled as $1\delta^{13}C_{PCE2}$) with progressively more positive $\delta^{13}C$ values (Damgaard et al., 2013; Puigserver et al., 2014). However, the decrease in the percentage of silt and the increase in the percentage of fine sand has reduced the degradation of PCE, which explains why PCE is increasingly lighter (−24.6‰ ± 0.1‰; Fig. 6a, label $1\delta^{13}C_{PCE3}$).

The increase in silt content, together with the existence of jointpoints that favor the accumulation of the PCE-DNAPL (Fig. 5, label $1PCE_3$, 32 μmol/L), has caused this compound to be significantly degraded, so that PCE is much heavier at this location (−22.6‰ ± 0.2‰; Fig. 6a, label $1\delta^{13}C_{PCE4}$) compared with the upper depths. Therefore, depths where there is an increase in the percentage of silt create a barrier to vertical migration of the PCE-DNAPL (as a result of capillary pressure). These compounds have accumulated in the past and currently present degradation halos (Fig. 6a, label $1PCE_1$, 102 μmol/L) consisting of a progressive decrease in PCE below the depth where there is a high concentration of PCE, an increase in the concentration of metabolites (as observed by Puigserver et al. (2013, 2016a, 2016b)), and isotope enrichment of PCE (Fig. 6a, in the depth range labeled as$1\delta^{13}C_{PCE2}$).

The substantial increase in the percentage of silts at borehole B-F1-UB in the CB-aquitard (Fig. 5, label 1S1) has favored the accumulation of another PCE pool that has migrated there by gravity through a microfracture as well as laterally through the textural contrasts (Fig. 5, label $1PCE_4$, 1.7 μmol/L), which accounts for the light isotopic composition of PCE at this depth in the borehole (−24.8‰ ± 0.1‰; Fig. 6a, label $1\delta^{13}C_{PCE5}$). Below this level, PCE has continued migrating mainly by molecular diffusion through the silts, where greater degradation of PCE (with a heavier isotopic composition) was detected in the borehole (Fig. 6a, depth range marked with the label $1\delta^{13}C_{PCE6}$, whose least negative value was −23.51‰ ± 0.1‰). Below 12.16 m, PCE was no longer detected because the initial PCE had already degraded completely. The pattern of variation in PCE concentrations seen in Fig. 6b (borehole B-F2-UB) is similar to the pattern in Fig. 6a (borehole B-F1-UB), but the former has lower concentrations because borehole B-F2-UB is located in the terminal part of the accumulated pool in B-F1-UB, as observed in label $2PCE_1$ (9.2 μmol/L; Fig. 5). In B-F2-UB, there was a lower mass of the accumulated PCE-DNAPL pool than in borehole B-F1-UB, as observed in label $2PCE_1$ (9.2 μmol/L; Fig. 5). This finding explains why below 10.68 m in this borehole, PCE is no longer detected in the CB-aquitard: The accumulated pool has also already degraded.

An increase in PCE concentrations was detected in B-F2-UB (Fig. 6b, label $2PCE_2$, 0.52 μmol/L) at the geological contact between the TZCMA and the MB-aquitard in the presence of interstratified levels of fine to medium gravels. At these levels, as previously mentioned, the PCE-DNAPL has tended to accumulate and to migrate laterally, but at the same time, these transition zones are ecotones where PCE has clearly been degraded to TCE (as observed in the isotopic composition of PCE: −22.5‰ ± 0.2‰; Fig. 6b, label $2\delta^{13}C_{PCE1}$). Although a part of the spilled PCE has accumulated in these gravel levels, and groundwater flow occurs along them accompanied by an associated contamination plume, the PCE-DNAPL free phase has continued to migrate by gravity through the subvertical microfractures and by molecular diffusion into both sides of the microfractures. This movement explains why the dissolved phase of PCE was detected at greater depths in the S4 and S12 piezometers, which are screened between 25 and 30 m deep (Table 1).

4.5.2. PCE metabolites and their isotopic composition in the aquitards

Fig. 6 also shows the results of TCE, cDCE and VC concentration profiles in the boreholes. A significant decrease in TCE concentrations in B-F1-UB occurred with increasing depth in the TZBA, where maximum values were recorded (e.g., sample labeled $1TCE_1$, with 7.2 μmol/L). Further down, within the upper portion of the CB-aquitard, most of the samples recorded values below the LOQ, except for the peak corresponding to the sample labeled $1TCE_2$ (0.07 μmol/L; Fig. 6a). Still further down, in the lower portion of the aquitard, starting with the sample labeled $1TCE_3$ (with a TCE concentration of 0.42 μmol/L; Fig. 6a), a trend of increasing TCE concentrations was observed (except for the sample labeled $1TCE_4$, where a minimum value was recorded, 0.13 μmol/L). The TCE concentration profile in borehole B-F2-UB was similar to that of B-F1-UB, with high values observed not only in the lower portion of the CB-aquitard, but also in the transition zone to the MB-aquitard (Fig. 6b), and even within the latter aquitard (Fig. 6b, labels $2TCE_1$ and $2TCE_2$, with 3.5 and 13.3 μmol/L, respectively). cDCE concentrations in B-F1-UB (Fig. 6a) were in general low and in many cases below the LOQ, with the exception of the TZBA and the lower portion of the CB-aquitard (where some peaks, although of low concentrations, were recorded). In B-F2-UB (Fig. 6a), in contrast to B-F1-UB, the number of samples with values below the LOQ was significantly lower. The general trend was a decrease in values until the base of the transition zone with the MB-aquitard, below which most of the recorded cDCE concentrations were below the LOQ. As for VC, it was detected in B-F1-UB with high concentrations (Fig. 6a) at almost all depths in the profile. Thus, average concentrations of 1.2 μmol/L were registered in the TZBA, and 0.51 μmol/L in the CB-aquitard (0.23 μmol/L considering the values above the LOQ and those below this limit as zero). A trend was observed with decreasing concentrations with depth (although alternating with zones where values were below the LOQ; Fig. 6a). In B-F2-UB (Fig. 6b), VC was below the LOQ in most of the profile, with the exception of a maximum concentration recorded in the upper part of CB-aquitard (label $2VC_1$, 3.05 μmol/L) and maximum values in the MB-aquitard.

Furthermore, Fig. 6 also displays the variation profiles for the $\delta^{13}C$ values of TCE in the aquitard porewater in the two boreholes. In B-F1-UB, concentrations were low, and even below the LOQ. For this reason, TCE $\delta^{13}C$ values could only be recorded in the TZBA and toward the base of the CB-aquitard. In both cases, the values became more negative with increasing depth (with TCE $\delta^{13}C$ values that decreased up to −30.3‰ ± 0.3‰ and −30.6‰ ± 0.2‰, respectively; Fig. 6a). In B-F2-UB, the low variability of the measured TCE $\delta^{13}C$ values stand out, except for the zone immediately above and below the geological contact between the TZCMA and the MB-aquitard, where the least negative value in the two boreholes within the two aquitards stands out (−28.9‰ ± 0.4‰, in Fig. 6b). In the case of cDCE and VC, their low concentrations did not allow $\delta^{13}C$ values to be determined.

The distribution of PCE metabolites in the CB-aquitard at B-F1-UB is shown in Fig. 6a and b. At the depth of the PCE-DNAPL pool in the surface contact between the TZBA and the CB-aquitard (Fig. 6a, label $1PCE_1$, 102 μmol/L), despite high concentrations of the parent compound, there was production of TCE (Fig. 6a, label $1TCE_1$, with 7.2 μmol/L). In fact, above the pool there is the mentioned biofilm, denoted as biodegradation halo by Puigserver et al. (2016a). However, the high PCE concentrations made it difficult for the degradation of the originally spilled PCE to have evolved toward a more advanced stage with the formation of metabolites with fewer

chlorine atoms, although in some cases it could take place (Zhao and He, 2019).

The decreased PCE concentrations below the dot labeled $1PCE_1$ (Fig. 6a, 102 μmol/L) coincide with decrease in TCE concentrations below dot labeled $1TCE_3$ (Fig. 6a), with a TCE concentration of 0.42 μmol/L. The depths where joint-points occurred and where, as mentioned above (see introduction of Section 4.5), PCE accumulated, showed a markedly increased TCE concentration. Thus, there was a

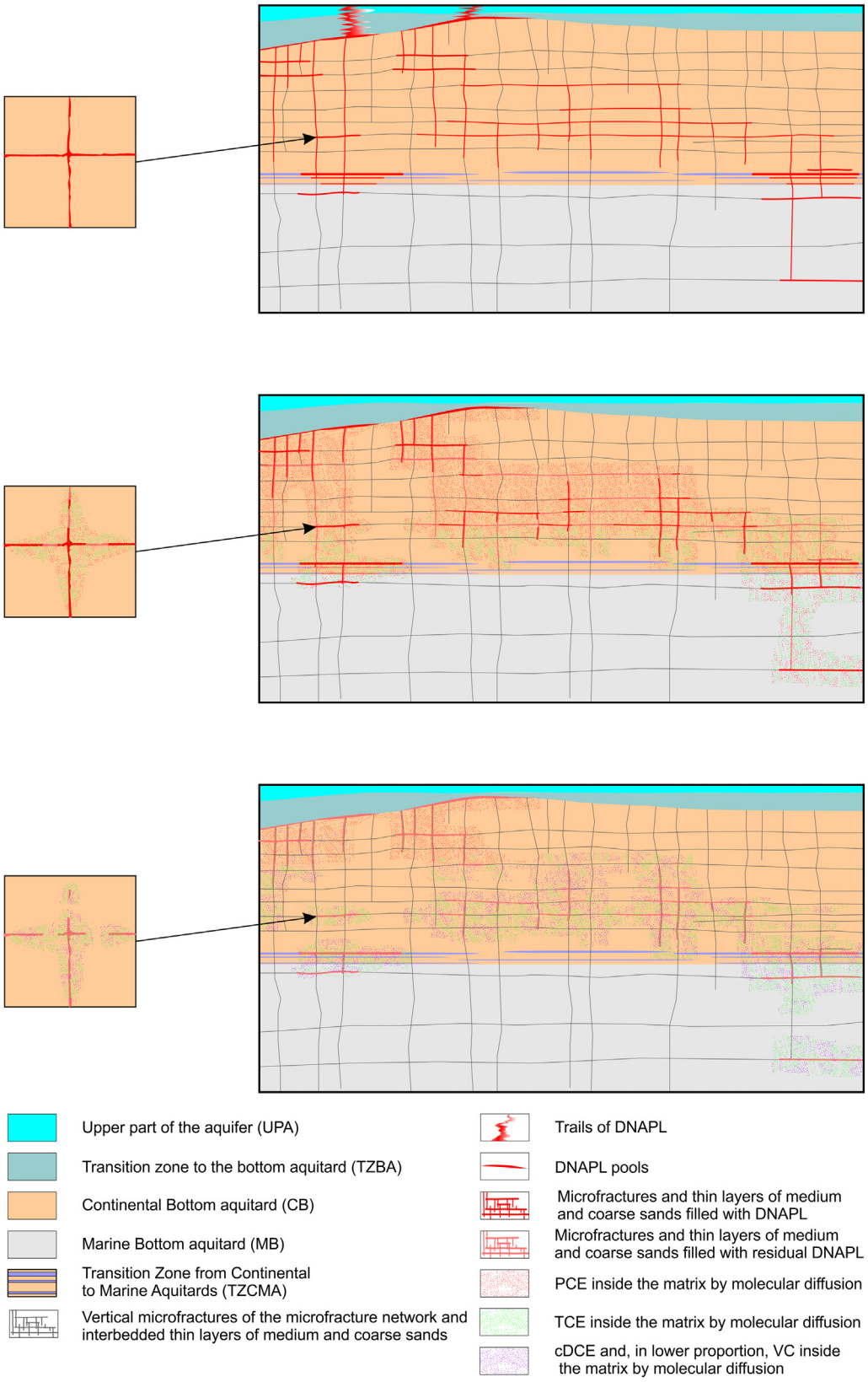

Fig. 7. Conceptual model of the migration of the PCE free phase and its evolution over time (through the orthogonal network of microfractures, bedding planes, joint-points, and thin layers of more conducive materials).

degradation halo (that results in a maximum of TCE of 0.07 μmol/L; Fig. 6a, $1TCE_2$) located above the depth of the maximum of PCE labeled $1PCE_3$ (32 μmol/L), similarly to what has been described by Puigserver et al. (2013, 2016a, 2016b). In addition, at this same depth in the case of B-F2-UB (Fig. 6b), the VC concentration was significantly increased (Fig. 6b, label $2VC_1$, 3.05 μmol/L). This phenomenon indicates the existence of a more advanced reductive dechlorination (Filippini et al., 2020) at depths where PCE is bioavailable.

Below the zone of the dot labeled $1PCE_4$ (Fig. 6a, 1.7 μmol/L), there was a progressive decrease in PCE up to 12.5 m. Below this depth, the PCE concentrations in the porewater were very low (and most of them lower than LOQ). These low PCE concentrations were accompanied by a progressive increase in TCE concentrations up to 17 m (Fig. 6a), the depth at which the borehole B-F1-UB ended. However, prior to the end of the borehole, there were points with decreased TCE accompanied by increased cDCE. These cDCE maxima and TCE minima formed degradation halos, as observed in the dot labeled $1cDCE_1$ (Fig. 6a, with a concentration of 0.075 μmol/L). These findings parallel a decrease in TCE at label $1TCE_4$ (0.13 μmol/L) and show that reductive dechlorination has existed (Puigserver et al., 2013, 2016a, 2016b).

Below 17 m in the lower part of the TZCMA (in B-F2-UB), the presence of the interstratified layers of medium gravels has allowed groundwater flow with dissolved PCE that in part penetrated into fine materials (see Section 4.5.1 and Fig. 6b, label $2PCE_2$, 0.52 μmol/L). This groundwater flow ensures a simultaneous supply of nutrients, electron donors, and other natural factors (see Section 4.6) that favor biotic reductive dechlorination (Puigserver et al., 2020). This is evidenced by the presence of TCE (Fig. 6b, label $2TCE_1$, 3.5 μmol/L), which from the point labeled $2\delta^{13}C_{TCE1}$ became increasingly heavier with depth (−31.3‰‰ ± 0.2‰; Fig. 6b) at both sides of the aforementioned interstratified layers, as well as by the presence of cDCE (Fig. 6b, label $2cDCE_1$, with 0.092 μmol/L), and VC at similar depths (Thouement et al., 2019).

The presence of metabolites at depths greater than those at which PCE is currently located demonstrates that PCE had reached these depths of the MB-aquitard in the past (Peter et al., 2011), and that what in the early times of the contamination episode had been a young source at this depth, currently has become an aged source (Seyedabbasi et al., 2012) that is evolving very slowly. Fig. 7 shows how the contamination has evolved over time. PCE has penetrated: i) as a free phase through the network of microfractures, bedding planes, and more conductive interstratified levels to great depths, and ii) by molecular diffusion into the matrix. PCE that is deeper in the matrix, and far from the detected free phase or residual-phase pools, has clearly degraded to TCE, and to a lesser extent to cDCE and VC. In fact, the depths where there was degradation of up to cDCE and VC are those where there is a supply of nutrients, contaminants, electron donors, and other substances (see Section 4.6) supplied by interbedded gravel levels. This finding indicates that to promote the biotic degradation of contaminants, the nutrient content and other substances in the aquitard should be at least increased (Wanner et al., 2016). In parallel, there was an increase in Fe at these depths, possibly as a consequence of the occurrence of Fe oxide mineral precipitates (see Section 4.3). This eventuality suggests that the degradation of PCE that has penetrated the matrix from microfractures is a consequence of the coupling of reactive abiotic and biotic processes (Entwistle et al., 2019; Puigserver et al., 2020), thus supporting the first working hypothesis.

4.6. Reductive dechlorination in the porewater with the presence of the *Dehalococcoides* genus and *Propionibacterium acnes*

Fig. 6a and b shows the richness of microbial communities within the aquitard and the presence or absence of microorganisms of the genus *Dehalococcoides* and *Propionibacterium acnes*. In the CB-aquitard, in borehole B-F1-UB, the maximum richness was recorded at the depth corresponding to the dot labeled $1R_1$ (Fig. 6a). This location coincides with the joint-point zone with the maximum PCE concentration (Fig. 5, label $1PCE_3$, 32 μmol/L), but where there was also a strong decrease in the concentration of this pollutant with depth (see Section 4.5). This high richness corresponded to neither the presence of *Dehalococcoides* spp. nor cDCE nor VC. This decrease in PCE, accompanied by the presence of a degradation halo from PCE to TCE (Fig. 6a, label $1TCE_4$, 0.13 μmol/L), indicates that dechlorinating microbial communities capable of surviving in the presence of high concentrations of PCE, but not belonging to the *Dehalococcoides* genus, are present in the medium (Dolinová et al., 2017). The presence of *P. acnes*, a bacterium related to the reductive dechlorination of chloroethenes (Chang et al., 2011), was detected at this depth (Fig. 6a). These findings support the second working hypothesis. By contrast, the maximum microbial richness indicated by the label $1R_2$ at the bottom of this CB-aquitard (Fig. 6a) coincided with a low PCE, an increase in TCE, and the presence of cDCE and *Dehalococcoides* spp. Thus, when the PCE concentration decreases, *Dehalococcoides* spp. are able to conduct reductive dechlorination at least up to cDCE (Zhao and He, 2019; Löffler et al., 2013). Therefore, this system has the potential to degrade chloroethenes in the aquitard (Manoli et al., 2012), confirming once again the second working hypothesis.

In B-F2-UB, *Dehalococcoides* spp. were detected at all depths, including the CB-aquitard, the TZCMA, and the MB-aquitard (Fig. 6b), in contrast to what was observed in B-F1-UB. The occurrence of *Dehalococcoides* in B-F2-UB could be related to a lower concentration of PCE in the porewater (even at the depth where the residual PCE pool was detected; Fig. 6b, label $2PCE_1$, 9.2 μmol/L). Moreover, the presence of *Dehalococcoides* spp. coincided with a higher TCE concentration, especially at the depth where the PCE pool was placed. Hence, reductive dechlorination mediated by *Dehalococcoides* spp. could be more effective at lower concentrations of PCE (Fig. 6b, label $2PCE_1$, 9.2 μmol/L). However, it is not excluded that *P. acnes* may have played a role at the depth of the point labeled $2PCE_1$ in this borehole (B-F2-UB).

At the upper part of the CB-aquitard, the richness of microbial communities in B-F2-UB increased with depth from its contact with the TZBA (Fig. 6b). This change accounts for the increase in TCE, cDCE, and VC concentrations compared with the concentrations in B-F1-UB and

Table 3
Physicochemical parameters and concentrations of the main redox-sensitive indicators measured in groundwater of the conventional piezometer S4.

Date	EC (μS/cm)	Eh (mV)	DO (mg/L)	NH_4^+ (mg/L)	NO_2^- (mg/L)	NO_3^- (mg/L)	Mn^{2+} (mg/L)	Fe^{2+} (mg/L)	SO_4^{2-} (mg/L)
Jul-10	622	−50	0.90	0.002	0.1	0.01	0.36	0.15	123
Mar-11	587	126	3.60	0.002	0.0004	0.05	0.011	0.12	38
Mar-12	1141	−145	0.28	0.002	0.0004	2.30	0.105	0.026	403.78
Nov-13	694	−33	0.18	0.002	0.0004	0.05	0.013	0.084	139
Oct-14	760	−92	0.2	0.002	0.0004	0.05	0.772	0.028	192
May-14	720	10	1.68	0.2	0.001	0.89	0.012	0.079	121
Jun-16	672	−220	0.06	0.14	0.5	11.74	1.21	0.05	300.33
Feb-17	887	−176	0.12	0.06	1.63	15.1	0.555	0.009	321
Jun-17	775	−164	0.1	0.002	0.07	0.05	0.237	0.028	269

Table 4
DO variations with depth in the multilevel piezometers of the Transition Zone to the Bottom Aquitard (TZBA) and in conventional piezometers S4 and S12.

Upper part of the TZBA	Port F1-6UB	6.3 m depth	6.47 mg/L DO	Port F2-6UB	6.6 m depth	4.74 mg/L DO
Interface zone between the TZBA and the CB-aquitard	Port F1-7UB	6.9 m depth	3.30 mg/L DO	Port F2-7UB	7.2 m depth	0.65 mg/L DO
Change from clearly oxidizing conditions in the shallower ports to lesser DO in the lower part of the TZBA						
Lower part of the MB-aquitard (interbedded conductive medium sands, groundwater flow occurs)	Conventional piezometer S4	25–30 m depth	0.06 to 3.60 mg/L DO			
	Conventional piezometer S12	25–30 m depth	0.80 to 3.45 mg/L DO			
Variations depend on the season of year for sampling. The minimum value in S4 is lower than in S12						

confirms that B-F2-UB presents greater chloroethene degradation because this borehole is in a more distant zone from the primary source of the PCE-DNAPL, located at the contact between the TZBA and the CB-aquitard (see Section 4.1). In addition, the gravel and sand interstratified layers in B-F2-UB in the TZBA provided the necessary nutrients, dissolved PCE, electron donors (dissolved organic carbon that acts as an energy source), and growth factors—substances naturally occurring that stimulate growth, proliferation, differentiation, and cellular healing—that *Dehalococcoides* spp. need to biodegrade chloroethenes (Fowler and Reinauer, 2013; Miura et al., 2015; Puigserver et al., 2016a). Furthermore, particulate organic matter in fine sands and silts between the more conductive layers also acts as an electron donor (Puigserver et al., 2014).

4.7. Groundwater chemistry in interstratified conductive layers within the MB-aquitard

Table 3 shows the main physicochemical parameters and redox-sensitive species measured in the conventional piezometer S4, screened between 25 and 30 m at the interstratified levels of medium sands (Section 2.2). Table 4 shows the variation in DO in the groundwater of the TZBA as well as the mentioned interstratified conductive layers within the MB-aquitard (piezometers S4 and S12).

EC did not vary significantly during the studied period: It ranged between 600 and 1100 μS/cm. The Eh (see Table 3) indicated a reducing character, and the DO was mostly below 1 mg/L.

The periods in which Eh values were more negative corresponded to the summer and winter seasons (especially in 2016 and 2017, respectively) because these are the driest periods (lower rainfall) based on the Mediterranean climate in the region. This seasonality is evidence that a hydraulic connection exists between the conductive interstratified levels in the MB-aquitard (piezometer S4) with the exterior (from where it is recharged by infiltration of part of the rainwater), which shows that there is groundwater flow along this zone (i.e., it is not stagnant groundwater, without flow). In this region, nitrate concentrations in aquifers are very high because the fields are fertilized with manure (see Section 2.1); in most cases, they are around 50 mg/L. In general, the redox conditions recorded at S4 were more reducing than at the conventional piezometer S12 (screened between the same depths as S4). The average Eh value recorded in S4 was −82.7 mV, with a range

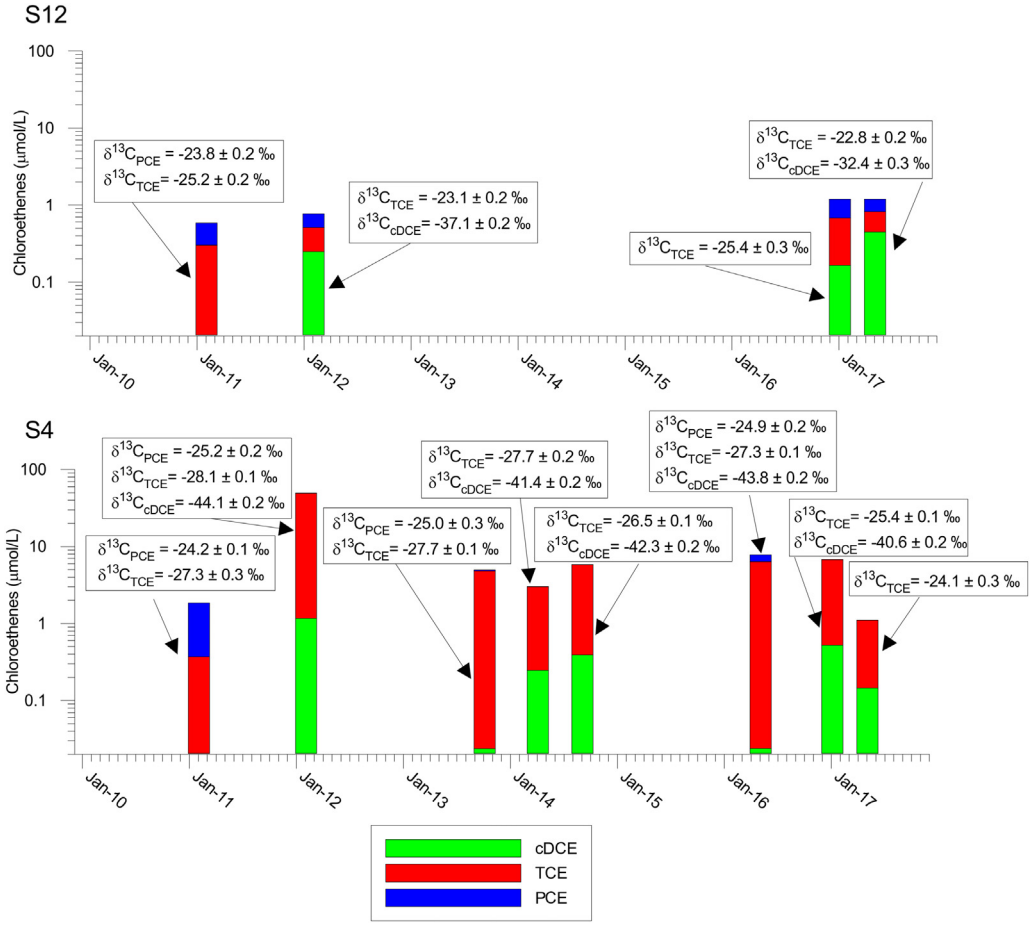

Fig. 8. Evolution of the accumulated concentrations of chloroethenes and their isotopic composition in the groundwater of conductive thin layers in the aquitard.

from −220 to 126 mV, whereas in S12 the average was −21 mV, and the range was from −70 to 135 mV. These predominant reducing conditions in S4 account for the low concentrations of nitrogen species as a consequence of denitrification occurring at that depth (Lasagna et al., 2015; Zhou et al., 2017).

Although concentrations of nitrogen species were low, the data in Table 3 indicate that during the summer and autumn–winter periods, concentrations of nitrate and ammonium increased, coinciding with the period during which fields are fertilized with manure. These data again confirm that there is a connection between this groundwater and the exterior. This was accompanied by an increase in the concentration of sulfate, so a significant part of this ion in these interstratified conductive layers has an agricultural origin (Jakóbczyk-Karpierz et al., 2017). The high levels of Mn and Fe in a reduced state, together with the high sulfate (showing that sulfate reduction did not occur), indicate that the previously mentioned reducing conditions prevailing in piezometer S4 vary between those corresponding to the redox zone of Mn reduction and Fe reduction.

Chloroethene concentrations in groundwater (Fig. 8) revealed that TCE and often cDCE concentrations were higher than the PCE concentrations, in contrast to what was observed in the TZBA-hydrostratigraphic unit (Puigserver et al., 2016a). This is in accordance with what was observed in the porewater of the TZCMA (see Section 4.5.1), where, although PCE was detected, TCE concentrations were higher. The progressive increase in TCE and cDCE concentrations in groundwater of S4 and S12 were not accompanied by isotope fractionation of cDCE. Although these compounds showed different isotopic compositions (Fig. 8), the isotopic shift between them remained fairly constant at both the S4 and S12 conventional piezometers. However, cDCE concentrations increased, indicating that degradation of TCE to cDCE probably took place. The following circumstances were present for this to occur: 1) groundwater flow supplying electron donors (dissolved and particulate organic matter, which acting as energy source), TCE acting as electron acceptor, nutrients and growth factors that dechlorinating microorganisms need; and 2) sufficiently reducing redox conditions (Table 3) for biotic reductive dechlorination of TCE to cDCE to take place. Piezometer S12 recorded an isotopically heavier PCE than S4 (−23.8‰ ± 0.2‰ and −25.2‰ ± 0.2‰, respectively). This is because PCE in S12 is a dissolved form proceeding from a PCE-DNAPL that, from the primary source (located at the TZBA-CB-aquitard interface; Fig. 2 and Section 4.1), has had to travel a longer path than in the case of S4 through the aquitard microfracture network to S12. There has been a longer residence time in the aquitard, and therefore more time degrading until reaching the conductive levels where S12 is situated (Fig. 2). This agrees with the fact that in S12, there are higher molar fractions of cDCE than TCE, while in S4 the molar fractions of TCE are higher than cDCE. Moreover, in S4 the isotopic compositions of TCE and cDCE were on average −27.14‰ ± 0.2‰ and −42.44‰ ± 0.2‰, respectively, which in both cases were lighter than in S12 (where they were on average −24.12‰ ± 0.2‰ and −34.75‰ ± 0.3‰, respectively), confirming that in S12 the currently degrading PCE had been in place in the aquitard longer than in the case of S4, and is therefore already isotopically heavier.

Taken together, these findings confirm that the source has aged but it has not been fully mineralized (Scheutz et al., 2010). Fig. 8 also shows how the maximum production of cDCE occurs in the summer, coinciding with Fe-reducing conditions (Chambon et al., 2013; Herrero et al., 2019).

5. Conclusions

Degradation in fractured aquitards occurs especially in the matrix adjacent to the orthogonal network of microfractures, bedding planes, and interstratified conductive layers. PCE has penetrated by molecular diffusion from the PCE-DNAPL present in this network. PCE degradation has occurred especially when the secondary PCE-DNAPL sources in the network have evolved to a mature state. The existence of textural heterogeneities at different depths within aquitards, especially at depths where there are contrasts between fine and coarse grain sizes, favors microbial development because these zones become ecotones. The biodegradation activity performed by *Dehalococcoides* (and also by *P. acnes*) in aquitards is incomplete. However, this activity, combined with the reactive abiotic degrading effect caused by Fe oxides present in these aquitards, ensures the total mineralization of chloroethenes. This is especially remarkable in the porewater of the host matrix of sediments on either side of microfractures. The existence of biodegradation and abiotic degradation of chloroethenes in the matrix of low hydraulic conductivity formations has important environmental implications because large amounts of these contaminants are stored in the pores of these formations. The mobilization of these contaminants is complicated because of the difficult accessibility of such contexts. The presence of degradation processes of chloroethenes at the matrix level favors a decrease in the mass of stored contaminants in case of complete mineralization of the parent PCE, which reduces back-diffusion of this compound caused by reverse concentration gradients, and thus the rebound effect. This lowering of the rebound effect has positive implications, because chloroethenes are highly recalcitrant compounds. However, when complete mineralization of the PCE parent compound does not occur, the formation of daughter products in the aquitard generates steep concentration gradients of these compounds between the aquitards and the high hydraulic conductivity layers. This triggers high back-diffusion fluxes of daughter products from the aquitard to these more conductive layers.

The ability of *Dehalococcoides* to biodegrade chloroethenes in the matrix adjacent to microfractures often contrasts with joint-point zones resulting from the intersection of microfractures, where high chloroethene concentrations can be toxic to *Dehalococcoides*. At these depths, biodegradation is often mediated by other microorganisms such as *P. acnes*. However, this biodegradation is not complete and does not result in total mineralization.

The above-mentioned textural contrasts often allow the occurrence of layers in which groundwater flow occurs and where: i) the dominant redox conditions are Fe reducing; ii) precipitation of iron oxides with sorbed Fe^{2+} ions is possible; and iii) there is a simultaneous supply of nutrients, electron donors, and acceptors, along with a supply of other compounds that microorganisms need to live. Together, these scenarios may favor the coupling of reactive abiotic and biotic degradation of chloroethenes. However, the dechlorination resulting from the coupling of reactive abiotic and biotic processes in aquitards is slow and limited by the need for an adequate supply of electron donors. Hence, for the remediation of this type of site, the implementation of strategies based on the use of combined reactive abiotic and biotic in situ methods could be an opportunity to solve one of the most important threats regarding environmental contamination caused by chlorinated solvents. This is a real challenge because aquitards are connected to aquifers in many hydrogeological contexts, especially in alluvial fan settings.

CRediT authorship contribution statement

Diana Puigserver: She carried out the VOC analyses in the porewater and groundwater, executed and testified the research boreholes, processed the data and wrote the article. She participated in the discussion meetings of the results obtained.

Jofre Herrero: He carried out the microbial and isotopic analyses. He participated in the joint discussion meetings of the results obtained.

Xènia Nogueras: She carried out the granulometry analysis and contributed to the sampling and pre-treatment of sediment samples.

Amparo Cortés: She carried out the pre-treatment, analysis, and interpretation of the results of Fe, Mn and organic carbon. She participated in the discussion meetings of the results obtained.

Beth L. Parker: The method of extraction and analysis of VOC in the porewater was designed and supervised by this co-author. She also supervised the final version of the article.

Elisabet Playà: She conducted the study and interpretation of results of the analysis of sediment samples by Scanning Electron Microscopy.

José M. Carmona: He participated in the execution of the research boreholes, in the testification, in the hydrodynamic and geochemical characterization of the medium, supervised the article and participated in the discussion meetings of the results obtained. He was also the principal investigator of the project that funded the research.

Declaration of competing interest

The authors declare that they have no known competing financial interests or personal relationships that could have appeared to influence the work reported in this paper.

Acknowledgments

We are indebted to the Catalan Water Agency and to the members of INTERFREN of Figueres and INTECSON S.L. of Reus for their support and cooperation while carrying out the field work. We should also like to thank Dr. Ivonne Nijenhuis (Helmholtz Centre for Environmental Research - UFZ, Leipzig-Germany) for her advice on microbial richness and the presence of the *Dehalococcoides* genus. We are grateful to the personnel of the Scientific and Technological Centres of the University of Barcelona for their help in analyzing the samples. We should also like to acknowledge the institution funding the research carried out within the following projects: CTM 2005-07824 and CGL 2008-02164/BTE (Spanish Ministry of Education).

Appendix A. Supplementary data

Supplementary data to this article can be found online at https://doi.org/10.1016/j.scitotenv.2021.151532.

References

Adamson, D.T., Chapman, S.W., Farhat, S.K., Parker, B.L., deBlanc, P., Newell, C.J., 2015. Characterization and source history modeling using low-k zone profiles at two source areas. Groundw. Monit. Remediat. 35 (2), 52–69.

Antoniou, K., Mamais, D., Pantazidou, M., 2019. Reductive dechlorination of trichloroethene under different sulfate-reducing and electron donor conditions. J. Contam. Hydrol. 226, 103519.

Bae, S., Lee, W., 2012. Enhanced reductive degradation of carbon tetrachloride by biogenic vivianite and Fe (II). Geochim. Cosmochim. Acta 85, 170–186.

Berns, E.C., Sanford, R.A., Valocchi, A.J., Strathmann, T.J., Schaefer, C.E., Werth, C.J., 2019. Contributions of biotic and abiotic pathways to anaerobic trichloroethene transformation in low permeability source zones. J. Contam. Hydrol. 224, 103480.

Bouwer, E.J., 1994. Bioremediation of chlorinated solvents using alternate electron acceptors. In: Norris, R.D., et al. (Eds.), Handbook of Bioremediation. Lewis Publishers, pp. 149–175.

Bradley M., Paul, 2003. History and ecology of chloroethene biodegradation: a review. Biorem. J. 7 (2), 81–109. https://doi.org/10.1080/713607980.

Bradley M., Paul, 2011. Reinterpreting the importance of oxygen-based biodegradation in chloroethene-contaminated groundwater. Monit. Rem. 31 (4), 50–55. https://doi.org/10.1111/j.1745-6592.2011.01344.x.

Bradley, P.M., Chapelle, F.H., 1997. Kinetics of DCE and VC mineralization under methanogenic and Fe (III)-reducing conditions. Environ. Sci. Technol. 31, 2692–2696.

Brown, G.H., Brooks, M.C., Wood, A.L., Annable, M.D., Huang, J., 2012. Aquitard contaminant storage and flux resulting from dense nonaqueous phase liquid source zone dissolution and remediation. Water Resour. Res. 48 (6).

Chambon, J.C., Bjerg, P.L., Scheutz, C., Bælum, J., Jakobsen, R., Binning, P.J., 2013. Review of reactive kinetic models describing reductive dechlorination of chlorinated ethenes in soil and groundwater. Biotechnol. Bioeng. 110 (1), 1–23.

Chang, Y.-C., Ikeutsu, K., Toyama, T., Choi, D., Kikuchi, S., 2011. Isolation and characterization of tetrachloroethylene-and cis-1, 2-dichloroethylene-dechlorinating propionibacteria. J. Ind. Microbiol. Biotechnol. 38, 1667–1677.

Chapelle, F.H., Bradley, P.M., 2004. Redox conditions and the reductive/oxidativebiodegradation of chlorinated ethenes in groundwater systems. Dehalogenation. Springer, Boston, MA, pp. 373–384.

Chapman, S.W., Parker, B.L., 2005. Plume persistence due to aquitard back diffusion following dense nonaqueous phase liquid source removal or isolation. Water Resour. Res. 41 (12), W12411.

Chapman, S.W., Parker, B.L., Sale, T.C., Doner, L.A., 2012. Testing high resolution numerical models for analysis of contaminant storage and release from low permeability zones. J. Contam. Hydrol. 136, 106–116.

Cheng, Z., Gao, B., Xu, H., Sun, Y., Shi, X., Wu, J., 2016. Effects of surface active agents on DNAPL migration and distribution in saturated porous media. Sci. Total Environ. 571, 1147–1154.

Cheremisinoff, N.P., 2017. Groundwater remediation: A practical guide for environmental engineers and scientists. John Wiley & Sons.

Cohen, R.M., Mercer, J.W., 1993. DNAPL site evaluation. C. K. Smoley, CRC Press, Boca Raton, Fla.

Culpepper, J.D., Scherer, M.M., Robinson, T.C., Neumann, A., Cwiertny, D., Latta, D.E., 2018. Reduction of PCE and TCE by magnetite revisited. Environ. Sci. Process. Impacts 20 (10), 1340–1349.

Cwiertny, D.M., Scherer, M.M., 2010. Chlorinated solvent chemistry: structures, nomenclature and properties. In situ remediation of chlorinated solvent plumes. Springer, New York, NY, pp. 29–37.

Damgaard, I., Bjerg, P.L., Bælum, J., Scheutz, C., Hunkeler, D., Jacobsen, C.S., Broholm, M.M., 2013. Identification of chlorinated solvents degradation zones in clay till by high resolution chemical, microbial and compound specific isotope analysis. J. Contam. Hydrol. 146, 37–50.

Dearden, R.A., Noy, D.J., Lelliott, M.R., Wilson, R., Wealthall, G.P., 2013. Release of contaminants from a heterogeneously fractured low permeability unit underlying a DNAPL source zone. J. Contam. Hydrol. 153, 141–155.

Dincutoiu, I., Górecki, T., Parker, B.L., 2003. A novel technique for rapid extraction of volatile organohalogen compounds from low permeability media. Environ. Sci. Technol. 37 (17), 3978–3984.

Dolinová, I., Štrojsová, M., Černík, M., Němeček, J., Macháčková, J., Ševců, A., 2017. Microbial degradation of chloroethenes: a review. Environ. Sci. Pollut. Res. 24 (15), 13262–13283.

Domenico, P.A., Schwartz, F.W., 1998. Vol. 506. Wiley, New York.

Duhamel, M., Mo, K., Edwards, E.A., 2004. Characterization of a highly enriched dehalococcoides-containing culture that grows on vinyl chloride and trichloroethene. Appl. Environ. Microbiol. 70 (9), 5538–5545.

Entwistle, J., Latta, D.E., Scherer, M.M., Neumann, A., 2019. Abiotic degradation of chlorinated solvents by clay minerals and Fe (II): evidence for reactive mineral intermediates. Environ. Sci. Technol. 53 (24), 14308–14318. https://doi.org/10.1021/acs.est.9b04665.

Fan, D., Bradley, M.J., Hinkle, A.W., Johnson, R.L., Tratnyek, P.G., 2016. Chemical reactivity probes for assessing abiotic natural attenuation by reducing iron minerals. Environ. Sci. Technol. 50 (4), 1868–1876.

Fang, H., Zhu, J., 2018. New approach for simulating groundwater flow in discrete fracture network. J. Hydrol. Eng. 23 (7), 04018025.

Fawad, M., Mondol, N.H., Jahren, J., Bjørlykke, K., 2010. Microfabric and rock properties of experimentally compressed silt-clay mixtures. Mar. Pet. Geol. 27 (8), 1698–1712.

Field, J.A., Sierra-Alvarez, R., 2001. Review of scientific literature on microbial dechlorination and chlorination of key chlorinated compounds. Department of Chemical & Environmental Engineering University of Arizona 37p.

Field, J.A., Sierra-Alvarez, R., 2004. Biodegradability of chlorinated solvents and related chlorinated aliphatic compounds. Rev. Environ. Sci. Biotechnol. 3 (3), 185–254.

Filippini, M., Parker, B.L., Dinelli, E., Wanner, P., Chapman, S.W., Gargini, A., 2020. Assessing aquitard integrity in a complex aquifer–aquitard system contaminated by chlorinated hydrocarbons. Water Res. 171, 115388.

Findlay, M., Smoler, D.F., Fogel, S., Mattes, T.E., 2016. Aerobic vinyl chloride metabolism in groundwater microcosms by methanotrophic and etheneotrophic bacteria. Environ Sci Technol 50, 3617–3625.

Fitch, M.W., Speitel, G.E., Georgiou, G., 1996. Degradation of trichloroethylene by methanol-grown cultures of methylosinus trichosporium OB3b PP358. Appl. Environ. Microbiol. 62 (3), 1124–1128.

Fjordbøge, A.S., Janniche, G.S., Jørgensen, T.H., Grosen, B., Wealthall, G., Christensen, A.G., Broholm, M.M., 2017. Integrity of clay till aquitards to DNAPL migration: assessment using current and emerging characterization tools. Groundw. Monit. Remediat. 37 (3), 45–61.

Fowler, T., Reinauer, K., 2013. Enhancing reductive dechlorination with nutrient addition. Remediat. J. 23 (1), 23–35.

Goldscheider, N., Hunkeler, D., Rossi, P., 2006. Microbial biocenoses in pristine aquifers and an assessment of investigative methods. Hydrogeol. J. 14 (6), 926–941.

Guilbaud, R., White, M.L., Poulton, S.W., 2013. Surface charge and growth of sulphate and carbonate green rust in aqueous media. Geochim. Cosmochim. Acta 108, 141–153.

Guilbeault, M.A., Parker, B.L., Cherry, J.A., 2005. Mass and flux distributions from DNAPL zones in sandy aquifers. Ground Water 43 (1), 70–86.

Hartog, H., Cho, J., Parker, B.L., Annable, M.D., 2010. Characterization of a heterogeneous DNAPL source zone in the borden aquifer using partitioning and interfacial tracers: residual morphologies and background sorption. J. Contam. Hydrol. 115 (1), 79–89.

He, Y.T., Wilson, J.T., Su, C., Wilkin, R.T., 2015. Review of abiotic degradation of chlorinated solvents by reactive iron minerals in aquifers. Groundw. Monit. Remediat. 35 (3), 57–75.

Herrero, J., Puigserver Cuerda, D., Parker, B.L., Carmona Pérez, J.M., 2021a. A new method for determining compound specific carbon isotope of chlorinated solvents in porewater. Groundwater Monitoring & Remediation 41 (3), 51–57. https://doi.org/10.1111/gwmr.12435.

Herrero, J., Puigserver, D., Nijenhuis, I., Kuntze, K., Carmona, J.M., 2019. Combined use of ISCR and biostimulation techniques in incomplete processes of reductive dehalogenation of chlorinated solvents. Sci. Total Environ. 648, 819–829.

Herrero, J., Puigserver, D., Nijenhuis, I., Kuntze, K., Carmona, J.M., 2021b. Key factors controlling microbial distribution on a DNAPL source area. Environ. Sci. Pollut. Res. https://doi.org/10.1007/s11356-021-15635-2.

Herrero, J., Puigserver, D., Nijenhuis, I., Kuntze, K., Parker, B.L., Carmona, J.M., 2021c. The role of ecotones in the dehalogenation of chloroethenes in alluvial fan aquifers. Environ. Sci. Pollut. Res. 1–14.

Holmes, V.F., He, J., Lee, P.K.H., Alvarez-Cohen, L., 2006. Discrimination of multiple dehalococcoides strains in a trichloroethene enrichment by quantification of their reductive dehalogenase genes. Appl. Environ. Microbiol. 72, 5877–5883. https://doi.org/10.1128/AEM.00516-06.

Hua, H., Yin, X., Fennell, D., Dyer, J.A., Landis, R., Morgan, S.A., Axe, L., 2021. Roles of reactive iron mineral coatings in natural attenuation in redox transition zones preserved from a site with historical contamination. J. Hazard. Mater. 420, 126600.

Huang, J., Goltz, M.N., 2015. Semianalytical solutions for transport in aquifer and fractured clay matrix system. Water Resour. Res. 51 (9), 7218–7237.

Huling, S.G., Weaver, J.W., 1991. Dense Nonaqueous Phase Liquids. US Environmental Protection Agency, Office of Research and Development and Office of Solid Waste and Emergency Response, Washington, DC March. Report No. EPA/540/4-91-002.

IGC, 1996. Mapa Geològic de Catalunya 1:25.000. No. 258-1-2 (77-22). Navata. Institut Cartogràfic de Catalunya. Servei Geològic de Catalunya, Barcelona.

ITGE, 1994. Report of the geological map of Spain (in Spanish), Sheet 258 (Figueres). Scale 1:50,000. ITGE (Geological and Mining Technological Institute), Madrid 84-7840-197-0.

Jakóbczyk-Karpierz, S., Sitek, S., Jakobsen, R., Kowalczyk, A., 2017. Geochemical and isotopic study to determine sources and processes affecting nitrate and sulphate in groundwater influenced by intensive human activity-carbonate aquifer Gliwice (southern Poland). Appl. Geochem. 76, 168–181.

Jugder, B.E., Ertan, H., Bohl, S., Lee, M., Marquis, C.P., Manefield, M., 2016. Organohalide respiring bacteria and reductive dehalogenases: key tools in organohalide bioremediation. Front. Microbiol. 7, 249.

Kim, E.-S., Nomura, I., Hasegawa, Y., Takamizawa, K., 2006. Characterization of a newly isolatedcis-1, 2-dichloroethylene and aliphatic compound-degrading bacterium, Clostridium sp. strain KYT-1. Biotechnol. Bioprocess Eng. 11, 553–556.

Krajmalnik-Brown, R., Hölscher, T., Thomson, I.N., Saunders, F.M., Ritalahti, K.M., Löffler, F.E., 2004. Genetic identification of a putative vinyl chloride reductase in dehalococcoides sp. Strain BAV1. Appl. Environ. Microbiol. 70, 6347–6351. https://doi.org/10.1128/AEM.70.10.6347-6351.2004.

Krzmarzick, M.J., Crary, B.B., Harding, J.J., Oyerinde, O.O., Leri, A.C., Myneni, S.C., Novak, P.J., 2012. Natural niche for organohalide-respiring chloroflexi. Appl. Environ. Microbiol. 78 (2), 393–401.

Lasagna, M., Franchino, E., De Luca, D.A., 2015. Areal and vertical distribution of nitrate concentration in Piedmont plain aquifers (North-western Italy). Engineering Geology for Society and Territory. 3. Springer, Cham, pp. 389–392.

Lee, M., Odom, J., Buchanan Jr., R., 1998. New perspectives on microbial dehalogenation of chlorinated solvents: insights from the field. Annu. Rev. Microbiol. 52, 423–452.

Löffler, F.E., Sun, Q., Li, J., Tiedje, J.M., 2000. 16S rRNA gene-based detection of tetrachloroethene-dechlorinating desulfuromonas and dehalococcoides species. Appl. Environ. Microbiol. 66, 1369–1374.

Löffler, F.E., Ritalahti, K.M., Zinder, S.H., 2013. Dehalococcoides and reductive dechlorination of chlorinated solvents. Bioaugmentation for groundwater remediation. Springer, New York, NY, pp. 39–88.

Lu, C., Broholm, M.M., Fabricius, I.L., Bjerg, P.L., 2014. Determination of matrix pore size distribution in fractured clayey till and assessment of matrix migration of dechlorinating bacteria. Bioremediat. J 18 (4), 295–308.

Luciano, A., Viotti, P., Papini, M.P., 2010. Laboratory investigation of DNAPL migration in porous media. J. Hazard. Mater. 176 (1), 1006–1017.

Malachowsky, K.J., Phelps, T.J., Teboli, A.B., Minnikin, D.E., White, D.C., 1994. Aerobic mineralization of trichloroethylene, vinyl chloride, and aromatic compounds by rhodococcus species. Appl. Environ. Microbiol. 60 (2), 542–548.

Manoli, G., Chambon, J.C., Bjerg, P.L., Scheutz, C., Binning, P.J., Broholm, M.M., 2012. A remediation performance model for enhanced metabolic reductive dechlorination of chloroethenes in fractured clay till. J. Contam. Hydrol. 131 (1–4), 64–78.

McCarty, P.L., 1997. Aerobic cometabolism of chlorinated aliphatic hydrocarbons. In: Ward, C.H., Cherry, J.A., Scalf, M.R. (Eds.), Subsurface Restoration. Ann Arbor Press Inc, Chelsea, Michigan, pp. 373–395.

McMurdie, P.J., Behrens, S.F., Müller, J.A., Göke, J., Ritalahti, K.M., Wagner, R., Spormann, A.M., 2009. Localized plasticity in the streamlined genomes of vinyl chloride respiring dehalococcoides. PLoS Genet. 5 (11), e1000714.

Mercer, J.W., Cohen, R.M., Noel, M.R., 2010. DNAPL site characterization issues at chlorinated solvent sites. In Situ Remediation of Chlorinated Solvent Plumes. Springer, New York, NY, pp. 217–280.

Miura, T., Yamazoe, A., Ito, M., Ohji, S., Hosoyama, A., Takahata, Y., Fujita, N., 2015. The impact of injections of different nutrients on the bacterial community and its dechlorination activity in chloroethene-contaminated groundwater. Microbes and environments 30 (2), 164–171. https://doi.org/10.1264/jsme2.ME14127.

National Research Council, 1999. Improving management of persistent of contaminants. Groundwater and soil cleanup. National Academic Press, Washington, DC, pp. 113–174.

Němeček, J., Marková, K., Špánek, R., Antoš, V., Kozubek, P., Lhotský, O., Černík, M., 2020. Hydrochemical conditions for aerobic/anaerobic biodegradation of chlorinated ethenes—a multi-site assessment. Water 12 (2), 322.

Nielsen, R.B., Keasling, J.D., 1999. Reductive dechlorination of chlorinated ethene DNAPLs by a culture enriched from contaminated groundwater. Biotechnol. Bioeng. 62, 160–165.

O'hara, S.K., Parker, B.L., Jørgensen, P.R., Cherry, J.A., 2000. Trichloroethene DNAPL flow and mass distribution in naturally fractured clay: evidence of aperture variability. Water Resour. Res. 36 (1), 135–147.

Pankow, J.F., Cherry, J.A., 1996. Dense Chlorinated Solvents and Other DNAPLs in Groundwater: History, Behavior, and Remediation. Waterloo Press, Ontario.

Parker, B.L., Gillham, R.W., Cherry, J.A., 1994. Diffusive disappearance of immiscible phase organic liquids in fractured geologic media. Ground Water 32 (5), 805–820.

Parker, B.L., Cherry, J.A., Chapman, S.W., Guilbeault, M.A., 2003. Review and analysis of chlorinated solvent dense nonaqueous phase liquid distributions in five Sandy aquifers. Vadose Zone J. 2, 116–137.

Parker, B.L., Chapman, S.W., Guilbeault, M.A., 2008. Plume persistence caused by back diffusion from thin clay layers in a sand aquifer following TCE source-zone hydraulic isolation. J. Contam. Hydrol. 102 (1), 86–104.

Peter, A., Held, T., Hüsers, N., Swartjes, F.A., 2011. Natural attenuation. dealing with contaminated sites. Springer, Dordrecht, pp. 979–1014.

Popat, S.C., Deshusses, M.A., 2011. Kinetics and inhibition of reductive dechlorination of trichloroethene, cis-1, 2-dichloroethene and vinyl chloride in a continuously fed anaerobic biofilm reactor. Environ. Sci. Technol. 45 (4), 1569–1578.

Puigserver, D., Carmona, J.M., Cortés, A., Viladevall, M., Nieto, J.M., Grifoll, M., Parker, B.L., 2013. Subsoil heterogeneities controlling porewater contaminant mass and microbial diversity at a site with a complex pollution history. J. Contam. Hydrol. 144 (1), 1–19.

Puigserver, D., Herrero, J., Torres, M., Cortés, A., Nijenhuis, I., Kuntze, K., Parker, B.L., Carmona, J.M., 2016a. Reductive dechlorination in recalcitrant sources of chloroethenes in the transition zone between aquifers and aquitards. Environ. Sci. Pollut. Res. 23, 18724–18741. https://doi.org/10.1007/s11356-016-7068-4.

Puigserver, D., Nieto, J.M., Grifoll, M., Vila, J., Cortés, A., Viladevall, M., Parker, B.L., Carmona, J.M., 2016b. Temporal hydrochemical and microbial variations in microcosm experiments from sites contaminated with chloromethanes under biostimulation with lactic acid. Bioremediat. J. 20 (1), 54–70.

Puigserver, D., Cortés, A., Viladevall, M., Nogueras, X., Parker, L.B., Carmona María, J., 2014. Processes controlling the fate of chloroethenes emanating from DNAPL aged sources in river–aquifer contexts. J. Contam. Hydrol. 168, 25–40. https://doi.org/10.1016/j.jconhyd.2014.09.005.

Puigserver, D., Herrero, J., Parker, B.L., Carmona, J.M., 2020. Natural attenuation of pools and plumes of carbon tetrachloride and chloroform in the transition zone to bottom aquitards and the microorganisms involved in their degradation. Sci. Total Environ. 712, 135679.

Reij, M.W., Kieboom, J., de Bont, J., Hartmans, S., 1995. Continuous degradation of trichloroethylene by Xanthobacter sp. strain Py2 during growth on propene. Appl. Environ. Microbiol. 61, 2936–2942.

Rezaei, A., Zhan, H., Zare, M., 2013. Impact of thin aquitards on two-dimensional solute transport in an aquifer. J. Contam. Hydrol. 152, 117–136.

Rivett, M.O., Dearden, R.A., Wealthall, G.P., 2014. Architecture, persistence and dissolution of a 20 to 45 year old trichloroethene DNAPL source zone. J. Contam. Hydrol. 170, 95–115.

Sabalowsky, A.R., Semprini, L., 2010. Trichloroethene and cis-1, 2-dichloroethene concentration-dependent toxicity model simulates anaerobic dechlorination at high concentrations: I. Batch-fed reactors. Biotechnol. Bioeng. 107 (3), 529–539.

Saiyari, D.M., Chuang, H.P., Senoro, D.B., Lin, T.F., Whang, L.M., Chiu, Y.T., Chen, Y.H., 2018. A review in the current developments of genus dehalococcoides, its consortia and kinetics for bioremediation options of contaminated groundwater. Sustain. Environ. Res. 28 (4), 149–157.

Sale, T.C., Zimbron, J.A., Dandy, D.S., 2008. Effects of reduced contaminant loading on downgradient water quality in an idealized two-layer granular porous media. J. Contam. Hydrol. 102 (1), 72–85.

Schaefer, C.E., Ho, P., Berns, E., Werth, C., 2018. Mechanisms for abiotic dechlorination of trichloroethene by ferrous minerals under oxic and anoxic conditions in natural sediments. Environ. Sci. Technol. 52 (23), 13747–13755.

Scheutz, Charlotte, Broholm M., Mette, Durant D., Neal, Weeth Begtrup, Eline, Jørgensen H., Torben, Dennis, Philip, Jacobsen S., Carsten, Cox E., Evan, Chambon C., Julie, Bjerg L., Poul, 2010. Field Evaluation of Biological Enhanced Reductive Dechlorination of Chloroethenes in Clayey Till. Environmental science & technology 44 (13), 5134–5141. https://doi.org/10.1021/es1003044.

Scheutz, C., Durant, N.D., Hansen, M.H., Bjerg, P.L., 2011. Natural and enhanced anaerobic degradation of 1, 1, 1-trichloroethane and its degradation products in the subsurface–a critical review. Water Res. 45 (9), 2701–2723.

Semprini, L., 1997. Strategies for the aerobic co-metabolism of chlorinated solvents. Curr. Opin. Biotechnol. 8, 296–308.

Seyedabbasi, M.A., Newell, C.J., Adamson, D.T., Sale, T.C., 2012. Relative contribution of DNAPL dissolution and matrix diffusion to the long-term persistence of chlorinated solvent source zones. J. Contam. Hydrol. 134, 69–81.

Shim, H., Ryoo, D., Barbieri, P., Wood, T., 2001. Aerobic degradation of mixtures of tetrachloroethylene, trichloroethylene, dichloroethylenes, and vinyl chloride by toluene-o-xylene monooxygenase of pseudomonas stutzeri OX1. Appl. Microbiol. Biotechnol. 56 (1), 265–269.

Thouement, H.A., Kuder, T., Heimovaara, T.J., van Breukelen, B.M., 2019. Do CSIA data from aquifers inform on natural degradation of chlorinated ethenes in aquitards? J. Contam. Hydrol. 226, 103520.

USEPA (2004). 2004 Edition of the Drinking Water Standards and Health Advisories. EPA 822-R-04-005. Office of Water U.S. Environmental Protection Agency. Washington DC. 20 pages.

Van Agteren, M.H., Keuning, S., Oosterhaven, J., 1998. Handbook on Biodegradation and Biological Treatment of Hazardous Organic CompoundsVol. 2. Springer Science & Business Media.

Verce, M.F., Ulrich, R.L., Freedman, D.L., 2001. Transition from cometabolic to growth-linked biodegradation of vinyl chloride by a Pseudomonas sp. isolated on ethene. Environ. Sci. Technol. 35, 4242–4251.

Verce, M.F., Gunsch, C.K., Danko, A.S., Freedman, D.L., 2002. Cometabolism of cis-1, 2-dichloroethene by aerobic cultures grown on vinyl chloride as the primary substrate. Environ. Sci. Technol. 36, 2171–2177.

Vogel, T.M., McCarty, P.L., 1985. Biotransformation of tetrachloroethylene to trichloroethylene, dichloroethylene, vinyl chloride, and carbon dioxide under methanogenic conditions. Appl. Environ. Microbiol. 49 (5), 1080–1083.

Walton, K., Manna, F., Unger, A., Parker, B.L., 2019. Advances in simulating multiphase flow in fractured porous media-a modeling study of DNAPL invasion and fate. AGUFM 2019, H41I–H1812I.
Wanner, P., Parker, B.L., Chapman, S.W., Aravena, R., Hunkeler, D., 2016. Quantification of degradation of chlorinated hydrocarbons in saturated low permeability sediments using compound-specific isotope analysis. Environ. Sci. Technol. 50 (11), 5622–5630.
Wanner, P., Parker, B.L., Chapman, S.W., Aravena, R., Hunkeler, D., 2017. Does sorption influence isotope ratios of chlorinated hydrocarbons under field conditions? Appl. Geochem. 84, 348–359.
Weatherill, J.J., Atashgahi, S., Schneidewind, U., Krause, S., Ullah, S., Cassidy, N., Rivett, M.O., 2018. Natural attenuation of chlorinated ethenes in hyporheic zones: a review of key biogeochemical processes and in-situ transformation potential. Water Res. 128, 362–382.
Weatherill, J.J., Krause, S., Ullah, S., Cassidy, N.J., Levy, A., Drijfhout, F.P., Rivett, M.O., 2019. Revealing chlorinated ethene transformation hotspots in a nitrate-impacted hyporheic zone. Water Res. 161, 222–231.
Weathers, L.J., Parkin, G.F., 1995. Metallic iron-enhanced biotransformation of carbon tetrachloride and chloroform under methanogenic conditions. Battelle Press, Columbus, OH (United States), pp. 117–122 No. CONF-950483. Ref. 42b.
Yang, Y.R., McCarty, P.L., 2000. Biologically enhanced dissolution of tetrachloroethene DNAPL. Environ. Sci. Technol. 34 (14), 2979–2984.
Yang, Y.R., McCarty, P.L., 2002. Comparison between donor substrates for biologically enhanced tetrachloroethene DNAPL dissolution. Environ. Sci. Technol. 36 (15), 3400–3404.
Yang, Z., Niemi, A., Fagerlund, F., Illangasekare, T., 2012. Effects of single-fracture aperture statistics on entrapment, dissolution and source depletion behavior of dense nonaqueous phase liquids. J. Contam. Hydrol. 133, 1–16.
Wiedemeier, T.H., Swanson, Moutoux, D.E., Gordon, E.K., Wilson, J.T., Wilson, B.H., Kampbell, D.H., Hansen, J.E., Haas, P., Chapelle, F.H., 1998. Technical protocol for evaluating natural attenuation of chlorinated solvents in ground water. Air Force Center for Environmental Excellence Technology Transfer Division Brooks Air Force Base, San Antonio, Texas, p. 396.
Yadav, Radheshyam, Pandey, Puneeta, 2018. A review on volatile organic compounds (VOCs) as environmental pollutants: fate and distribution. Intern. J. Plant Environ 4 (2), 14–26. https://doi.org/10.18811/ijpen.v4i02.2.
Yang, M., Annable, M.D., Jawitz, J.W., 2017. Field-scale forward and back diffusion through low-permeability zones. J. Contam. Hydrol. 202, 47–58.
Yu, S., Lee, P.K., Hwang, S.I., 2015. Groundwater contamination with volatile organic compounds in urban and industrial areas: analysis of co-occurrence and land use effects. Environ. Earth Sci. 74 (4), 3661–3677.
Zhao, S., He, J., 2019. Reductive dechlorination of high concentrations of chloroethenes by a dehalococcoides mccartyi strain 11G. FEMS Microbiol. Ecol. 95 (1), fiy209.
Zhou, W., Xia, L., Yan, X., 2017. Vertical distribution of denitrification end-products in paddy soils. Sci. Total Environ. 576, 462–471.